

Eduarda Pedruzzi da Silva

**Generation of a multi-wavelength Brillouin
erbium fiber laser with frequency spacing
versatility**

Vitória - ES

2022

Eduarda Pedruzzi da Silva

Generation of a multi-wavelength Brillouin erbium fiber laser with frequency spacing versatility

Dissertation submitted to the Postgraduate Program in Electrical Engineering from the Technological Center of the Federal University of Espirito Santo, as a partial requirement for obtaining a Master's Degree in Electrical Engineering focused on Telecommunication.

Federal University of Espirito Santo

Technological Center

Postgraduate Program in Electrical Engineering

Supervisor: Dr. Carlos Eduardo Schmidt Castellani

Co-supervisor: Dr. Arnaldo Gomes Leal-Junior

Vitória - ES

2022

Ficha catalográfica disponibilizada pelo Sistema Integrado de
Bibliotecas - SIBI/UFES e elaborada pelo autor

P371g Pedruzzi da Silva, Eduarda, 1997-
Generation of a multi-wavelength Brillouin erbium fiber
laser with frequency spacing versatility / Eduarda Pedruzzi da
Silva. - 2022.
70 f. : il.

Orientador: Carlos Eduardo Schmidt Castellani.
Coorientador: Arnaldo Gomes Leal-Junior.
Dissertação (Mestrado em Engenharia Elétrica) -
Universidade Federal do Espírito Santo, Centro Tecnológico.

1. Stimulated Brillouin Scattering. 2. Fiber Laser. 3. Non
linear optics. 4. Multi-wavelength fiber laser. 5. Brillouin fiber
laser. 6. Brillouin frequency shift. I. Schmidt Castellani, Carlos
Eduardo. II. Gomes Leal-Junior, Arnaldo. III. Universidade
Federal do Espírito Santo. Centro Tecnológico. IV. Título.

CDU: 621.3

Eduarda Pedruzzi da Silva

Generation of a multi-wavelength Brillouin erbium fiber laser with frequency spacing versatility

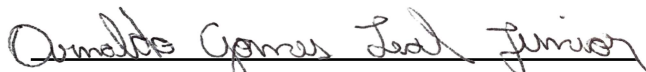
Dissertation submitted to the Postgraduate Program in Electrical Engineering from the Technological Center of the Federal University of Espírito Santo, as a partial requirement for obtaining a Master's Degree in Electrical Engineering focused on Telecommunication.

Dissertation approved. Vitória - ES, August 19, 2022:



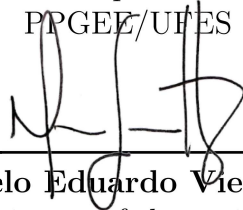
Dr. Carlos Eduardo Schmidt Castellani

Supervisor
PPGEE/UFES



Dr. Arnaldo Gomes Leal-Junior

Co-supervisor
PPGEE/UFES



Dr. Marcelo Eduardo Vieira Segatto

Member intern of the review board
PPGEE/ UFES



Dr. Shirley Peroni Neves Cani

Member extern of the review board
IFES

Vitória - ES

2022

To the memory of my Grandmother.

Acknowledgements

First, I thank God for yet another achievement. For He sustains my steps and makes me go beyond what I imagined arriving. And also to Our Lady for all intercession.

I would like to thank my family, my mother Maria and my father Valentin, and all my friends, especially Isadora and Rudson, for all their care and support for me. I am so grateful that you are part of my life.

I thank my friends and colleagues from the research group, especially Letícia and Fabiana, for the partnership, help, and for listening to all my doubts since I started working at LabTel. The journey was more fun having you by my side. Thank you to all the teachers of the Labtel group, with you I learned a lot and I hope to become a co-worker with some of you.

I thank the Graduate Program in Electrical Engineering at the Federal University of Espírito Santo. I acknowledge funding received from Petróleo Brasileiro S. A. - PETROBRAS (2017/00702-6), the research project of Fundação de Amparo à Pesquisa e Inovação do Espírito Santo (FAPES) "PRONEM" (88336650) and the funding received from Conselho Nacional de Desenvolvimento Científico e Tecnológico - CNPq/Brazil (130013/2020-0) for the realization of this research.

Finally, I thank my supervisors Carlos Eduardo and Arnaldo for all their patience, guiding me during my research, always being available to help me, for motivating me during all this time, and for showing me the best way forward.

"Search endlessly, fight 'til we're free
Fly past the edge of the sea
No bended knee
No mockery
Somehow we still carry on"

Avenged Sevenfold

Abstract

This dissertation proposes the production of a multi-wavelength laser, all in fiber, with different frequency spacings, using a non-linear effect, stimulated Brillouin scattering (SBS), combined with the use of an erbium doped fiber amplifier (EDFA). In a dual loop cavity configuration and 25km Non-Zero Dispersion-Shifted Fiber (NZDSF) fibers as the gain medium.

Lasers were first observed in the 1960s and are considered one of the significant technological advances of the 20th century. Many different laser systems have been developed and tested and have been used in a variety of applications. Optical fiber lasers and amplifiers have been attached much attention from the scientific community. But it was only in 1980, after a significant reduction in propagation losses and with the development of EDFA's, which made it possible to transport light over tens of kilometers of distance, that this technology has grown exponentially. In fact, despite the advances made, there is still a margin for this technology to progress, the biggest challenge being to improve performance, and overcoming some limiting factors, highlighting, the early appearance of non-linear effects, such as Raman scattering and Brillouin scattering, which cause the loss of incident power and cause the fading of the transmitted information. During the studies of these non-linear effects, several advantages and ways were found to combine them with the gain of the light beam and use them as amplifiers and generators, using different arrangements and techniques.

Multi-wavelength lasers (MWL) came to the fore after the development of wave division multiplexing (WDM) technology, which allows more channels to be carried on a single medium. The nonlinear Brillouin effect has a small frequency shift, about 10 GHz in silica, and a relatively low threshold power for generating the effect, in addition to being stable at room temperatures and tunable narrow linewidth frequency scheme, all of which make the multi-wavelength Brillouin laser (MWBL) hot spot on research, as it is easy to cascade and transmit all waves within the same communication band. It can also be produced entirely in optical fiber, which confers reliability, efficiency, excellent quality of the modal beam, low maintenance and they are compact structures. Combining these qualities, multi-wavelength Brillouin fiber lasers (MWBFL) can be used in various applications, such as sensing and dense wave division multiplexing (DWDM).

To implement this dissertation, a pump source with a narrow linewidth, about 1 kHz, was used, which allowed reached a low power threshold, approximately 1 mW, necessary to stimulate the non-linear effect in the fiber. For the choice of the Brillouin gain medium, three fibers with different characteristics were tested and the one that presented the best performance in terms of power threshold, frequency shift, and amplification was chosen, NZDSF of 25 km. For linear gain medium, an erbium-doped fiber (EDF), 10 m long,

pumped with a light source at 1474 nm was chosen. Finally, for laser cascading generating multiple wavelengths, three configurations were used that made it possible to increase the frequency spacing by up to three times the silica standard, approximately 9.08 GHz for the single array, 19.56 GHz for the double array, and 29.12 GHz for the triple frequency spacing.

Keywords: SBS, Nonlinear optics, Fiber lasers, Multi-wavelength fiber laser, Brillouin fiber laser, Brillouin frequency shift, Low threshold.

Resumo

Esta dissertação propõe a produção de um laser de múltiplos comprimentos de onda, todo em fibra, com diferentes espaçamentos de frequência, utilizando de um efeito não-linear, espalhamento estimulado de Brillouin (SBS), combinado como uso de um amplificador de fibra dopada com érbio (EDFA). Em uma configuração de cavidade de laço duplo e fibras Non-Zero Dispersion-Shifted Fiber (NZDSF) de 25km como meio de ganho.

Lasers foram observados pela primeira vez na década de 60, e são considerados um dos grandes avanços tecnológicos do século XX. Muitos sistemas diferentes de laser foram desenvolvidos e testados, sendo utilizada nos últimos anos em diversas aplicações. Os lasers e amplificadores em fibra ótica têm sido tema de grande atividade científica. Mas só em 1980, após significativa redução das perdas de propagação e com o desenvolvimento dos EDFA's, que possibilitaram transportar luz por dezenas de quilômetros de distância, que esta tecnologia recebeu forte impulso. Na realidade, apesar dos avanços obtidos, ainda existe uma margem de progressão desta tecnologia sendo o maior desafio melhorar o desempenho, ultrapassando alguns fatores limitadores. Destacando, o surgimento precoce de efeitos não-lineares, tais quais espalhamento Raman e espalhamento Brillouin, que provocam a perda de potência incidente e causam o esvanecimento da informação transmitida. Durante os estudos desses efeitos não lineares, foram encontradas diversas vantagens e formas de aliá-los ao ganho do feixe de luz e usá-los como amplificadores e geradores, fazendo uso de diferentes arranjos e técnicas.

Os lasers com múltiplos comprimentos de onda (MWL) se destacaram após o desenvolvimento da tecnologia de multiplexação por divisão de onda (WDM), que permite que mais canais sejam transportados em um único meio. O efeito não-linear Brillouin possui um deslocamento em frequência pequeno, cerca de 10 GHz em sílica, e uma potência limiar para geração do efeito relativamente baixa, além de ser estável em temperaturas ambientes e permitir a manipulação do espaçamento de frequência, tudo isso torna o laser Brillouin com múltiplos comprimentos de onda (MWBL) alvo de muita pesquisa, pois há uma facilidade em cascadear e transmitir todas as ondas dentro da mesma banda de comunicação. Podendo ainda ser produzido todo em fibra ótica, o que confere confiabilidade, eficiência, excelente qualidade de feixe modal, baixa manutenção e o fato de serem compactos. Aliando essas qualidades, os lasers Brillouin em fibra com múltiplos comprimentos de onda (MWBFL) podem ser utilizados em diversas aplicações, como sensoriamento e multiplexação por divisão de ondas densas (DWDM).

Para a realização dessa dissertação, foi usado uma fonte de bombeio com largura de linha estreita, cerca de 1 kHz, o que permitiu que fosse atingido um baixo limiar de potência, aproximadamente 1 mW, necessário para estimular o efeito não linear na fibra. Para a escolha do meio de ganho Brillouin, foram testadas três fibras com características

diferentes e escolhida a que apresentou o melhor desempenho quanto ao limiar de potência, deslocamento de frequência e amplificação, uma fibra com o zero de dispersão deslocado (NZDSF) de 25 km. Para meio de ganho linear, foi escolhida uma fibra dopada com érbio (EDF), 10 m de comprimento, bombeada com uma fonte de luz em 1474 nm. E por fim, para o cascadeamento do laser gerando múltiplos comprimentos de onda, foram empregues três configurações que possibilitaram aumentar o espaçamento de frequência em até três vezes do padrão em sílica, aproximadamente 9.08 GHz para o arranjo simples, 19.56 GHz para o duplo e 29.12 GHz para o triplo.

Palavras-chave: SBS, Ótica não linear, Lasers em fibra, Laser de múltiplos comprimentos de onda, Laser em fibra Brillouin, Deslocamento Brillouin, Baixo limiar de potência

List of Figures

Figure 1 – Schematic of a multimode step-index fiber and a graded-index fiber . . .	21
Figure 2 – The principle of total internal reflection in the optical fiber.	22
Figure 3 – The phenomena of absorption.	23
Figure 4 – The scattering of light by particles.	24
Figure 5 – Schematic of optical dispersion. a) Modal dispersion, b) Chromatic dispersion, and c) Waveguide dispersion.	26
Figure 6 – The radiation loss. a) Macro bending loss, and b) Micro banding loss. .	26
Figure 7 – Energy level diagrams illustrating a) absorption, b) spontaneous emission, and c) stimulated emission.	27
Figure 8 – Schematic setup of a simple erbium-doped fiber amplifier and energy diagram of erbium in 1480 nm.	29
Figure 9 – Schematic of Rayleigh, Brillouin, and Raman peaks in optical fiber (YÜCEL et al., 2017).	35
Figure 10 – Experimental laser setup: BP: Brillouin pump, FUT: fiber under test, OSA: Optical Spectrum Analyzer.	47
Figure 11 – Laser output power as a function of the pump power for a output coupling ratio of 90% for all three FUT.	48
Figure 12 – Output laser stability analysis for a coupling ratio of 90 % and under a pump power of 14 mW.	48
Figure 13 – Threshold as a function of the output coupling ratio for tests using all three FUT.	49
Figure 14 – Efficiency as a function of the output coupling ratio for tests using all three FUT.	50
Figure 15 – Optical spectra at the laser output for all three FUT used as the gain media.	50
Figure 16 – Experimental setups for multi-wavelength ring cavity Brillouin fiber laser with a single frequency spacing configuration.	51
Figure 17 – Experimental setups for multi-wavelength ring cavity Brillouin fiber laser with a double frequency spacing configuration.	52
Figure 18 – Experimental setups for multi-wavelength ring cavity Brillouin fiber laser with a triple frequency spacing configuration.	53
Figure 19 – Optical spectrum of the single Brillouin frequency spacing MWBEFL at the BP wavelength of 1565.8 nm and power of 1 mW. Here, the EDFA 1 pump power was 169.4 mW. Moreover, the frequency spacing between two adjacent wavelengths is 0.084 nm.	54

Figure 20 – Optical spectra generated with EDFA pump power values of 115.5 mW, 142.5 mW, 194.4 mW, 250.3 mW, and 277.2 mW. Here we adopt a BP power of 1 mW at 1550 nm.	55
Figure 21 – Optical spectra generated with EDFA pump power values of 115.5 mW, 142.5 mW, 194.4 mW, 250.3 mW, and 277.2 mW. Here we adopt a BP power of 1 mW at 1565 nm.	55
Figure 22 – Optical spectra generated with BP power values of 1 mW, 4 mW, and 14 mW. Here we adopt a EDFA pump power of 169 mW.	56
Figure 23 – Number of generated Brillouin Stokes lines within a range of 30 dB against the variations in EDFA pump power for BP wavelengths at 1565.8 nm and 1550.0 nm. Here we adopt a BP of 1 mW.	57
Figure 24 – Number of generated Brillouin Stokes lines within a range of 30 dB against the variations in EDFA pump power for BP powers of 1 mW, 4 mW, and 14 mW. Here we adopt all BP wavelengths at 1565.8 nm. . .	57
Figure 25 – Optical spectrum of the double Brillouin frequency spacing MWBEFL at the BP wavelength of 1565.8 nm, and power of 1 mW obtained at the output 1 (odd Stokes wavelengths). Here, the pump powers of EDFA 1 and EDFA 2 were both 336.5 mW. In addition, the frequency spacing between two adjacent wavelengths is 0.16 nm.	58
Figure 26 – Optical spectrum of the double Brillouin frequency spacing MWBEFL at the BP wavelength of 1565.8 nm, and power of 1 mW obtained at the output 2 (even Stokes wavelengths). Here, the pump powers of EDFA 1 and EDFA 2 were both 336.5 mW. Also, the frequency spacing between two adjacent wavelengths is 0.16 nm.	59
Figure 27 – Optical spectrum of the triple Brillouin frequency spacing MWBEFL at the BP wavelength of 1565.8 nm, and power of 1 mW. Here, the pump powers of EDFA 1 and EDFA 2 were both 336.5 mW. Further, the frequency spacing between two adjacent wavelengths is 0.24 nm. . .	60

List of abbreviations and acronyms

BP	Brillouin Pump
BGS	Brillouin Gain Spectrum
DCF	Dispersion Compensating Fiber
DWDM	Dense Wave Division Multiplexing
EDF	Erbium-Doped Fiber
EDFA	Erbium Doped Fiber Amplifier
FUT	Fiber Under Test
HNLF	Highly Non-Linear Fiber
IR	Infrared Region
ISI	Inter-Symbol Interference
LASER	Light Amplification by Stimulated Emission of Radiation
MMF	Multi-Mode Fiber
MWBEFL	Multi-Wavelength Brillouin–Erbium Fiber Laser
MWBFL	Multi-Wavelength Brillouin Fiber Laser
MWBL	Multi-Wavelength Brillouin Laser
MWL	Multi-Wavelength Laser
NZDSF	Non-Zero Dispersion-Shifted Fiber
OSA	Optical Spectrum Analyzer
OSNR	Optical Signal-to-Noise Ratio
SBS	Stimulated Brillouin Scattering
SMF	Single-Mode Fiber
SRS	Stimulated Raman Scattering
SWBFL	Single Wavelength Brillouin Fiber Laser
TLS	Tunable Laser Source
WDM	Wave Division Multiplexing

List of symbols

ϕ_c	Critical angle
n	Index of refraction
V	V-parameter
λ	Wavelength
P	Polarization
$\chi^{(i)}$	Susceptibility
E	Electric field
N	Density of dipole moment
α_p	Polarizability
Δ_ϵ	Dielectric constant
γ_e	Electrostrictive constant
Δ_ρ	Fluctuation in density
Δ_p	Fluctuation in pressure
ω_{ac}	Acoustic wave frequency
ω_L	Incident lighth frequency
\mathbf{F}_s	Stokes frequency
\mathbf{F}_{as}	Anti-stokes frequency
v_a	Acoustic velocity
ν_B	Brillouin shift
τ	Phonon lifetime
Γ	Phonon decay rate
P_{cr}	Critical power (Threshold)
A_{eff}	Effective area

L_{ef}	Effective length
α	Optical loss
γ_{pol}	Polarization factor
g_B	Brillouin gain spectrum
$\Delta\nu_B$	Full-width at half maximum
p_{12}	Longitudinal elasto-optic coefficient
γ	SBS efficiency
α	Non-linear coefficient

Contents

1	INTRODUCTION	18
1.1	Optical Fibers	19
1.1.1	Fiber characteristics	20
1.1.2	Fiber modes	22
1.1.3	Fiber losses	23
1.2	Fiber Lasers	27
1.2.1	Multi-wavelength fiber laser	30
1.2.2	Nonlinear Fiber Laser	31
1.3	Objectives	32
1.4	Contributions	33
1.5	Dissertation Structure	33
2	BRILLOUIN SCATTERING	34
2.1	Light scattering	34
2.2	Spontaneous Brillouin scattering	36
2.2.1	Brillouin frequency shift	39
2.3	Stimulated Brillouin scattering	40
2.3.1	Electrostriction	41
2.3.2	Brillouin threshold	43
2.3.3	Brillouin gain	44
3	ALL FIBER BRILLOUIN LASER	46
3.1	Experimental Setup	46
3.2	Results and Discussions	47
3.2.1	Laser Output Power	47
3.2.2	Threshold and Efficiency	48
3.2.3	Brillouin spectrum	49
4	MULTI-WAVELENGTH BRILLOUIN FIBER LASERS	51
4.1	Experimental setup	51
4.2	Results	53
4.2.1	Single frequency spacing Brillouin erbium fiber laser	53
4.2.2	Double frequency spacing Brillouin erbium fiber laser	56
4.2.3	Triple frequency spacing Brillouin erbium fiber laser	58
5	CONCLUSION	61

BIBLIOGRAPHY 62

1 Introduction

The properties of fibers as active media for lasers explains why fiber lasers have become one of the most popular choices for both academia and industry. This is particularly due to their excellent beam quality provided by the waveguide, robustness against mechanical vibrations, high average powers achievable, compact structures and low levels of intracavity losses (JAUREGUI; LIMPET; TÜNNERMANN, 2013). All these characteristics are required by many industrial (LACRAZ et al., 2015), security systems (SPRANGLE et al., 2015) and scientific applications (HU; JACKSON; HUDSON, 2015). Most types of fiber lasers are produced either from rare earth doped fibers (DIGONNET, 2001), fiber Bragg gratings (GILES, 1997), parametric amplification (XING et al., 2017), and also nonlinear effects such as nonlinear polarization rotation effect (FENG; TAM; WAI, 2006a), four-wave mixing (FRIEDLI et al., 2013), and stimulated Raman and Brillouin Scattering (FREUDIGER et al., 2014; OTTERSTROM et al., 2018).

The Brillouin fiber laser was first reported in 1976 (HECHT, 2004) and have remained an active topic of study since then due to important features, such as a narrow linewidth, low threshold power when compared to other types of amplifiers, and simple experimental configurations. Brillouin lasers and amplifiers can be found in many different applications, for example, including random fiber laser (ZHANG et al., 2018), Brillouin fiber-optic sensors (DONG, 2021), pulsed lasers (BERGLER et al., 2020), high-power lasers (DAJANI et al., 2010), and multi-wavelength laser (WANG et al., 2013a).

The nonlinear effect called Stimulated Brillouin Scattering (SBS) is the result of the interaction between an incident pump light and the phonons in a medium of gain, as the optical fiber. This interaction gives rise to backward propagating frequency-shifted light, with a specific shift (AGRAWAL, 2000). The Brillouin-shift is about to 0.1 nm at silica fiber. Brillouin fiber lasers are particularly interesting due to simple, low-cost setup, excellent conversion efficiency, fixed wavelength spacing, linewidth narrowing, and low threshold power (DIAMANDI; ZADOK, 2019). Because of this, has become a research hot spot in recent years owing to their promising use in a variety of fields, such as distributed fiber sensor (MARINI et al., 2017; MIZUNO et al., 2019), Dense wavelength division multiplexing (DWDM) and coherent optical communications (PELUSI; INOUE; NAMIKI, 2019; AL-MASHHADANI; AL-MASHHADANI; GOKTAS, 2019a) and multiwavelength Brillouin fiber lasers (MWBFL) (XUEFANG et al., 2019; XU; YUAN; ZHANG, 2018; LIU et al., 2020). This characteristic has been successfully employed in the generation of MWBFL because when changing the single wavelength Brillouin fiber lasers (SWBFL's) setup to dual-ring cavity setup and begin to generate the n - order Stokes lines signals, these are equally spaced at the Brillouin - shift. Therefore, multiwavelength lines are generated

in the same communication band, that provides the use on the diverse applications. But the stability in a time of wavelength and linewidth in SWBFL are difficult to control because of depending on characteristics pumped laser, gain medium, room temperature, and experimental configurations. And the line number in MWBFL and the flatness of output spectra is was hard due to the same problems as aforementioned, also because of the necessity to high amplification to overcome the cavity loss and more produced setup.

However, due to limited gain achieved by these nonlinear phenomena, the capacity and the efficiency of the produced laser were relatively low. A linear gain of erbium-doped fiber (EDF) were integrated with nonlinear Brillouin gain in the same laser cavity to enhance the laser performance. The new hybrid laser cavity is denoted by multi-wavelength Brillouin–Erbium fiber laser (MWBEFL) ([AGRAWAL, 2000](#)). In spite of the new hybrid laser cavity have an advantage in terms of capacity, efficiency, low threshold power and high induced gain, other limitations are considered such as laser tunability and very narrow channel spacing wavelength of 11 GHz (0.1 nm) that limits these lasers application in optical communication systems ([PENG et al., 2013](#)). Laser tunability issue were enhanced by many researchers using various techniques ([ZHANG; ZHAN; XIA, 2007](#); [AL-MASHHADANI; AL-MASHHADANI; GOKTAS, 2019b](#); [AL-MASHHADANI; AL-MASHHADANI; GOKTAS, 2020](#)). On the other side, more effort has been reported by many researchers to enlarge the laser line wavelength spacing. Although these configurations enable the generation of multi-wavelength fiber laser with different Brillouin frequency spacings, in most cases, these configurations are complex, requiring sophisticated amplification schemes with long fiber spools and high Brillouin pump (BP) powers. In this perspective, and focusing on the development of cost and energy-efficient pump sources, are experimentally demonstrate, the generation of the cascaded MWBEFLs with a low threshold, and a compact all-fiber setup with low loss, single, double, and triple frequency spacing configurations.

1.1 Optical Fibers

Daniel Colladon and Jacques Babinet first demonstrated the guiding of light by reflection for different refractive index, the principle that makes fiber optics possible, in Paris in the early 1840s ([HECHT, 1999](#)). In 1854, John Tyndall demonstrated to the Royal Society that light could be conducted through a curved stream of water, proving that a light signal could be bent ([F.R.S., 1854](#)). The phenomenon responsible for guiding light in optical fibers became known as total internal reflection ([AGRAWAL, 2012](#)). Although the idea of using arrays of transparent rods was patented in the 1920s ([BAIRD, 1927](#)), the use of glass fibers become practical only in the 1950s, when Dutch scientist Abraham Van Heel reported on imaging bundles of clad fibers. He covered a bare fiber with a transparent cladding of a lower refractive index. This protected the fiber reflection surface from outside distortion and greatly reduced interference between fibers ([HEEL, 1954](#)).

At the time, the greatest obstacle to a viable use of fiber optics for communications purposes was in achieving the lowest signal loss, the losses were approximately 1000 dB/Km (KAPANY, 1967). In the next decade, all efforts were directed to reduce this value. In 1964, Charles Kao and George Hockham, of Standard Communications Laboratories in England, demonstrated theoretically, that light loss in existing glass fibers could be decreased dramatically by removing impurities (KAO; HOCKHAM, 1966). Following the earlier suggestion, in 1970 the loss of optical fiber was reduced to below 20 dB/km (KAPRON; KECK; MAURER, 1970). Finally, in 1978 was achieved the loss of 0.2 dB/km at 1.55 μm , applying the Modified Chemical Vapor Deposition (MCVD) method and using germanium instead of titanium as the core dopant (MIYA et al., 1979). This fact was essentially responsible for the birth of a new era in the telecommunication field. This introductory chapter is intended to provide an overview of the fiber characteristics.

1.1.1 Fiber characteristics

An optical fiber geometry description is a circular dielectric waveguide that can transport optical energy and information. The fiber consists of a central core of a refractive index n_1 surrounded by a concentric cladding with a slightly lower refractive index (0.1 - 1%) n_2 and a protective coating. To confine the optical signal in the core, the refractive index of the core must be greater than that of the cladding. The boundary between the core and cladding may either be abrupt, where the refractive index is constant in both mediums, in step-index fiber or the refractive index of the core decreases gradually, in graded-index fiber. Figure 1, shows schematically the cross-section and refractive-index profile of a two kinds of fibers. The core and cladding typically are both made of silica glass (SiO_2) with index-modifying dopants added during the fabrication process. To increase a refractive index in n_1 fit dopants such as germanium dioxide (GeO_2) and phosphorus pentoxide (P_2O_5), while the cladding is doped materials such as boron and fluorine that cause the inverse effect. A protective coating, of cushioning material, commonly acrylate, is used to reduce cross-talk between adjacent fibers and the loss-increasing micro bending that occurs when fibers are pressed against rough surfaces. Silica is so widely used because of its outstanding properties, in particular its potential for extremely low propagation losses and its amazingly high mechanical strength against pulling and even bending (AGRAWAL, 2000).

The refractive index is a way of measuring the light bending ability in a material. It determines how much the path of light is bent or refracted when entering a material, as well as the critical angle for total internal reflection. For comprehension, a typical single-mode fiber (SMF) used for telecommunications has a cladding made of pure silica, with an index of 1.444 at 1.5 μm , and a core of doped silica with an index around 1.4475 (PASCHOTTA, 2008). The larger the index of refraction, the slower light travels in that

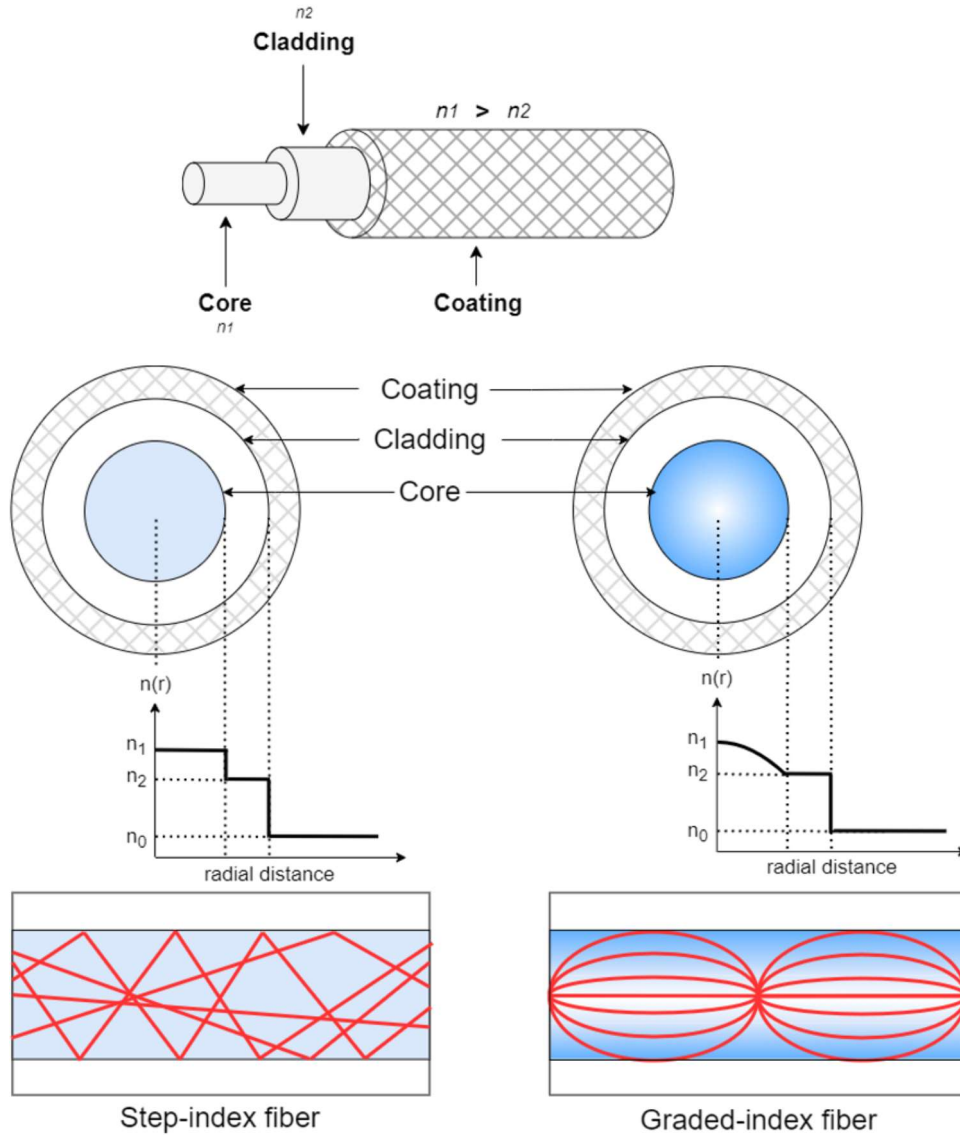


Figure 1 – Schematic of a multimode step-index fiber and a graded-index fiber

medium, that is meaning the most optical fiber is weakly guiding ([GLOGE, 1971](#)).

The phenomenon responsible for guiding light in optical fibers is known as total internal reflection. The phenomenon occurs if the angle of incidence is greater than a certain limiting angle, called the critical angle. In general, takes place at the boundary between two transparent media when a ray of light in a medium with a higher index of refraction (n_1) approaches the other medium (n_2) at an angle of incidence greater than the critical angle, then the refracted beam will be reflected entirely back into the core. In an optical fiber, the light travels through the core by constantly reflecting from the cladding because the angle of the light is always greater than the critical angle, for this the light wave can travel great distances ([SNYDER; LOVE, 2012](#)). Figure 2 presents an illustration of the principle of total internal reflection in the optical fiber.

In physics, the critical angle is described with respect to the normal line. In fiber

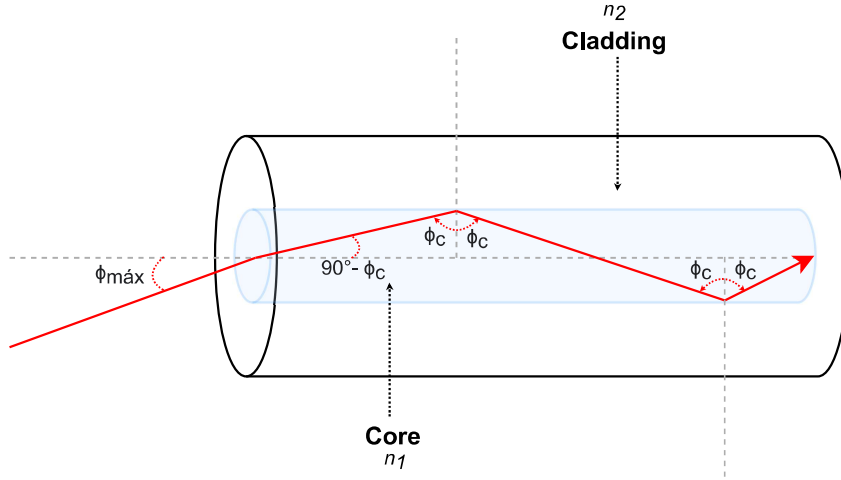


Figure 2 – The principle of total internal reflection in the optical fiber.

optics, the critical angle is described with respect to the parallel axis running down the middle of the fiber. Therefore, the fiber-optic critical angle = (90 degrees - physics critical angle). The critical angle in a fiber can be calculated using the Equation 1.1:

$$\phi_c = \sin^{-1} \left(\frac{n_2}{n_1} \right) \quad (1.1)$$

1.1.2 Fiber modes

Since the core has a higher index of refraction than the cladding, the light will be confined to the core if the angular condition for Total Internal Reflectance is met. The fiber geometry and composition determine the discrete set of electromagnetic fields, or fiber modes, which can propagate in the fiber. A mode is a way for the Electro-Magnetic field to satisfy the boundary conditions imposed by the physical structure of the fiber, such that the field patterns at different positions along the fiber's length remain the same (AGRAWAL, 2000).

There are two broad classifications of modes: radiation modes and guided modes. Radiation modes carry energy out of the core; the energy is quickly dissipated. Guided modes are confined to the core, and propagate energy along the fiber, can allow transporting information and power. The fiber can be split into the guided mode, like a single mode fiber (SMF) and a multi-mode fiber (MMF). The principal difference between the two types is the core size. For MMF, the core radius is typically 25-100 μm while the SMF presents a core radius of less than 5 μm . Single-mode fibers only support one mode, whereas in multi-mode fibers even thousands of modes are supported (AGRAWAL, 2000). The frequency normalized or V-parameter, so-called, determines the number of modes that are achieved by step-index fibers. The V-parameter is defined by Equation 1.2:

$$V = k_0 a (n_2^2 - n_1^2)^{1/2} \quad (1.2)$$

where $k_0 = 2\pi/\lambda$, a is the core radius, and λ is the wavelength of light. For a step-index fiber, Equation 1.3 presents the number of modes (N_m) inside the fiber.

$$N_m = \frac{V^2}{2} \quad (1.3)$$

For a fiber to be single mode it is necessary to fabricate it with a V value lower than 2.405.

1.1.3 Fiber losses

As mentioned previously, one of the main traits of optical fibers is their capacity to guide light with shallow loss, which can be below 0.2 dB/km at a wavelength of 1550 nm, for the silica types. Fiber loss or also called attenuation loss is a measure of the amount of light loss between input and output of the system. Losses in the optical fiber can be categorized into intrinsic losses depending whether the loss is caused by intrinsic characteristics, comprising absorption loss, dispersion loss, and scattering loss caused by structural defects. And, categorized as extrinsic losses caused by operating conditions, contains coupling loss, and radiation loss.

The absorption loss is related to the material composition and fabrication process of fiber. Although the fiber glasses are extremely pure, some impurities still remain as residues after purification resulting in the absorption, Figure 3. The phenomenon is explained by the dissipation of optical power on fiber and depends on the wavelength and impurities concentration for the amount of absorption (OKOSHI, 2012). The two types of absorption losses as explained below.

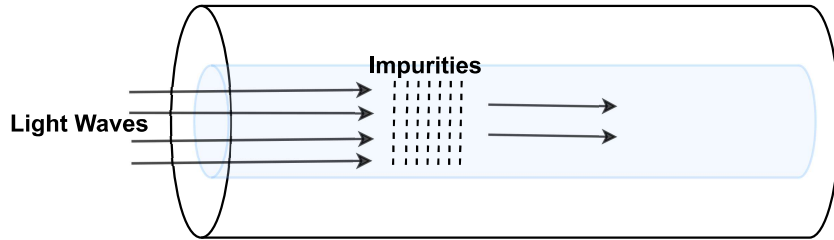


Figure 3 – The phenomena of absorption.

Intrinsic absorption occurs in the ultraviolet region, it happens due to the electronic absorption band. Basically, a photon interacts with an electron it is excited to a higher energy level and results in absorption. The characteristic vibration frequency of atomic bonds results in absorption loss in the infrared region (IR). An example of such an

interaction is the IR absorption band of SiO_2 . However, in the wavelength regions of interest to optical communication ($0.8\text{-}0.9\ \mu\text{m}$ and $1.2\text{-}1.5\ \mu\text{m}$), IR absorption tails make negligible contributions. The electromagnetic field and the interaction of vibration bonds is the main cause of intrinsic absorption. Extrinsic absorption is more relevant and common than intrinsic loss. They are the outcome of impurities in the fiber material during manufacturing, such as iron, nickel, and chromium, due to the transition of metal ions to higher energy levels. However, there are techniques for production to reduce impurity levels below 1 part per million (ppm). As an example, 1 ppm of Fe^{2+} would lead to a loss of $0.68\ \text{dB/km}$ at $1.1\ \mu\text{m}$. This shows the necessity of ultrapure fibers, where there are already developed techniques for reducing losses due to metallic ions to very low by refining the glass mixture to an impurity level below 1 part per billion (ppb) (OKOSHI, 2012).

Scattering losses occur due to the interaction of light with density fluctuations within a fiber, in a way that removes energy in the directional propagating wave and transfers it to other directions, Figure 4. Density changes are produced when optical fibers are manufactured. There are two main types of scattering: linear scattering and nonlinear scattering. For linear scattering, the amount of light power that is transferred from a wave is proportional to the power in the wave. It is characterized by having no change in frequency in the scattered wave. Rayleigh scattering is the main type of linear scattering, that arises from local microscopic fluctuations in density, which causes local random fluctuations in the refractive index. As light travels in the core, it interacts with the silica particles in the core. These elastic collisions between the light wave and the silica molecules result in Rayleigh scattering. If the scattered light maintains an angle that supports forward travel within the core, no attenuation occurs. If the light is scattered at an angle that does not support continued forward travel, the light is diverted out of the core and attenuation occurs. Some scattered light is reflected back toward the light source (BOYD, 2020).

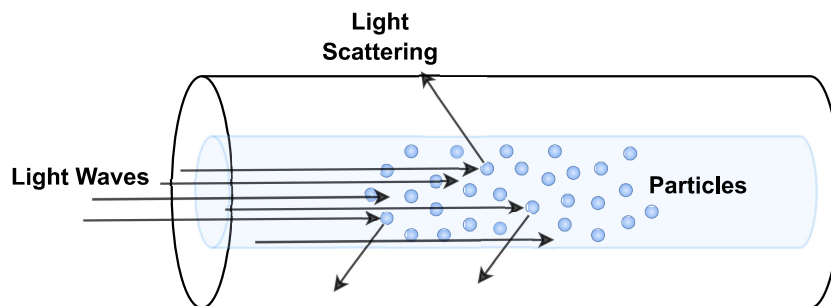


Figure 4 – The scattering of light by particles.

In opposition, nonlinear scattering is accompanied by a frequency shift of the light. Nonlinear scattering is caused by the high values of the power of an optical field inside

the fiber. Nonlinear scattering causes significant power to be scattered in all directions. In fiber optics, a perturbation in the longitudinal direction is more efficient in the process of approaching light. The scattering transverse to the longitudinal axis of the optical fiber can be neglected (JR; FRAGNITO, 2006). There are two categories of inelastic non-linear effects: Stimulated Raman Scattering (SRS) and Stimulated Brillouin Scattering (SBS). Both phenomena can be understood on a quantum-mechanical level as the annihilation of a photon from a pump field and the generation of a Stokes photon at a lower frequency and a phonon. The main difference between them is that SRS is associated with optical phonons, whereas acoustic phonons participate in SBS (FABELINSKII, 2012).

In general, light scattering is classified with elastic when the frequency of radiation scattering is the same as the frequency of incident light. If there is a difference between the frequencies the scattering process is called inelastic (BOYD, 2020). In both cases, when the intensity of the incident field is small enough to not provoke changes in the optical properties of the medium, is called linear, and when the intensity of the incident field is greater than the intensity of the atomic field, the optical properties undergo strong changes, so the process is classified as non-linear (HECHT, 2015).

Dispersion is the spreading out of a light pulse in time as it propagates down the fiber. As each light pulse broadens and overlaps with a neighboring pulse, Inter-symbol interference (ISI) occurs which makes the pulses indistinguishable at the receiver (FOX, 2002). Dispersion in optical fiber includes modal dispersion, chromatic dispersion, and waveguide dispersion. Modal dispersion occurs in multimode fibers, is due to the propagation delay differences between modes within a multimode fiber. This is shown in Figure 5.a. Each mode enters the fiber at a different angle and thus travels at different paths in the fiber. Since each mode ray travels a different distance as it propagates, the ray arrives at different times at the fiber output. So the light pulse spreads out in time which can cause signal overlapping.

Chromatic dispersion is the pulse spreading that arises because the velocity of light through a fiber depends on its wavelength, and can occur on mono-mode and multi-mode fibers, as represented in Figure 5.b. Waveguide dispersion is a problem in single-mode fibers. It is caused by the fact that some light travels in the fiber cladding compared to most light travels in the fiber core. Since fiber cladding has a lower refractive index than fiber core, the light ray that travels in the cladding travels faster than that in the core. While the difference in refractive indices of single mode fiber core and cladding are minuscule, they can still become a factor over greater and superior distances to those where the chromatic dispersion becomes significant, shown in Figure 5.c.

Radiation loss occurs when the fiber is curved. There are two types of radiative losses: micro bending losses and macro bending losses. Macro bending happens when the fiber is bent into a large radius of curvature relative to the fiber diameter, while micro

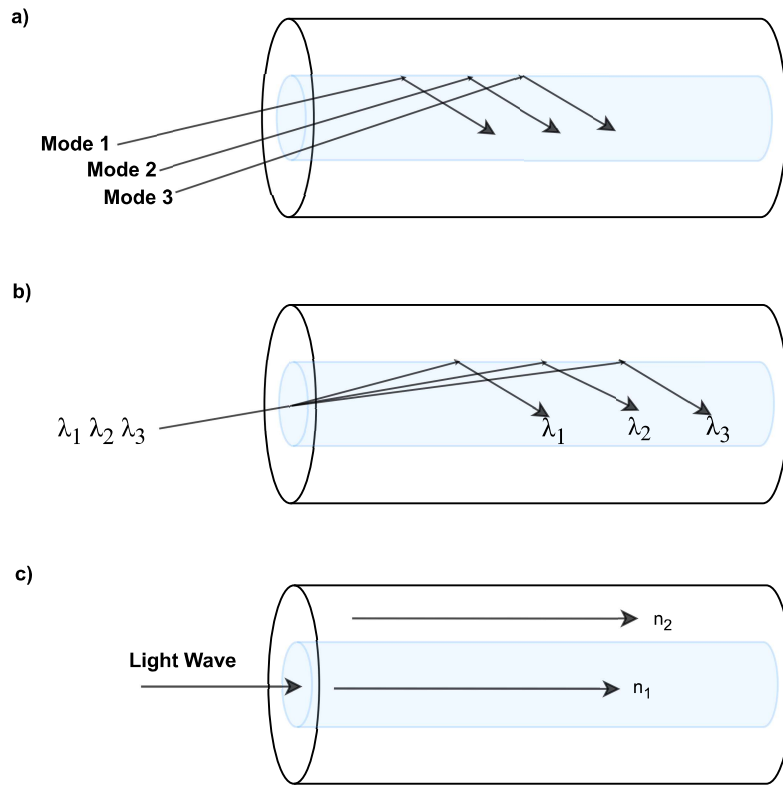


Figure 5 – Schematic of optical dispersion. a) Modal dispersion, b) Chromatic dispersion, and c) Waveguide dispersion.

bendings are the small-scale bends in the core-cladding interface. Figure 6 represents the two types of radiation loss. The coupling loss in fiber optics refers to the power loss that occurs when coupling light from one optical device to another, encompassing the splicing losses and connector losses.

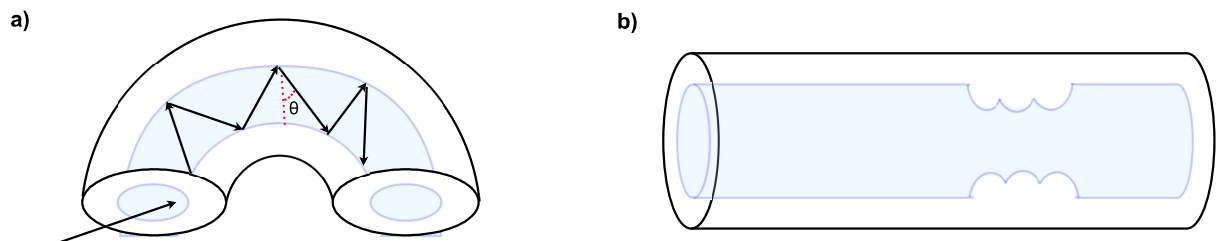


Figure 6 – The radiation loss. a) Macro bending loss, and b) Micro bending loss.

In long distance telecommunication systems, single-mode fibers are preferably used because on a multi-mode fiber each different mode travels with a different group velocity causing dispersion and therefore signal distortion at high-repetition rates. Their reduced core sizes also make SMFs ideal hosts for the generation of nonlinear effects even when using moderate optical powers. MMFs are mainly used for short-distance optical fiber communications where the effects of dispersion are not very significant.

1.2 Fiber Lasers

The laser is among the most important inventions of the twentieth century. Since their development by Theodore Maiman in 1960, laser has made possible a countless number of scientific, medical, industrial, and commercial applications (HECHT, 2004). The word *Laser* is an acronym for Light Amplification by Stimulated Emission of Radiation. They represent a class of light sources in the visible, near-ultraviolet or near/middle infrared spectral range, which increase or amplify light signals after those signals have been generated by other means. These processes include stimulated emission and optical feedback, that is usually provided by mirrors to feed the light back into the amplifier for the continued growth of the developing beam. At present, a variety of laser sources is available such as, gas lasers (ZHOU et al., 2018), dye lasers (MOZAFFARI; FARMANI, 2019), solid-state lasers: are usually divided into two categories, they can be either bulk (SHAO et al., 2020) or fiber-based lasers (TRAXER; KELLER, 2020), and semiconductor lasers (ZHANG et al., 2021), covering a wide spectral range. (SILFVAST, 2004).

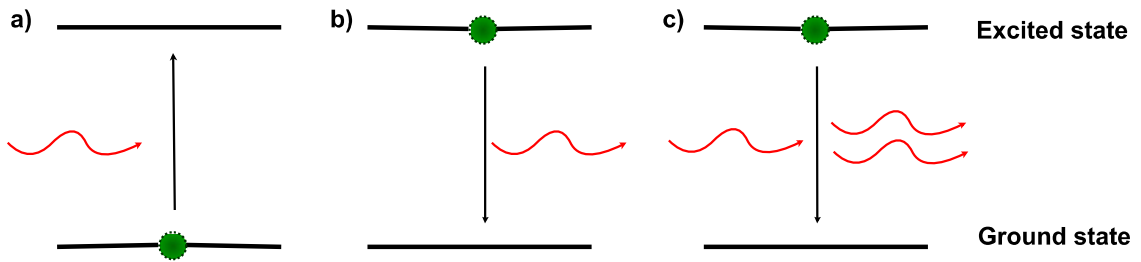


Figure 7 – Energy level diagrams illustrating a) absorption, b) spontaneous emission, and c) stimulated emission.

The atomic structure of any material, be it solids, liquids, gases, or plasma is made up of protons, neutrons, and electrons. When the light is launched inside in fiber, the electrons interact with this energy from light (photon), and then the absorption, spontaneous emission, and stimulated emission are the three related energy conversion processes. Optical energy is converted to internal energy when a photon is absorbed, the energy may cause an electron in an atom to go from a lower to a higher energy level, this process is known as absorption and is represented in Figure 7a). If an atom is in an excited state, it may spontaneously decay into a lower energy level after some time, the energy is conserved when the electron decays to the lower level and is converted into the form of a photon, which is emitted in any direction, phase, and electromagnetic polarization, Figure 7b). Stimulated emission, is when a photon interacts with an excited atom and causes the emission of a second photon or phonon (heat energy) having the same frequency, phase, polarization, and direction, Figure 7c). In effect, the incoming radiation is amplified (SALEH; TEICH, 2019). In resume, when are two energy states, a

ground, and an excited state, the electrons excited can amplify light, and the electrons in the fundamental state absorb light, which brings them back to the excited state and emit energy. The amplification can be achieved when most of the atoms are in the upper energy level, this condition is called population inversion.

In a fiber laser the active medium is the core of the fiber, which can be doped or not. Commonly, this fiber is a single-mode type and is made of silica. The pump beam is launched longitudinally along the fiber length and may be guided either by the core itself as occurs for the laser mode, for conventional single-mode fiber laser, or by an inner cladding around this core, double-clad fiber laser (HECHT, 2015).

A fiber laser, following the principle of fiber construction, contains at least one core region of the highest refractive index, in which is launched the light pump. This region is surrounded by one or more cladding regions of progressively decreasing refractive index, which serve to confine light rays within the core, as a mirror. Light incident on cladding regions penetrates and becomes trapped in the core region that reflects the light along the fiber, this phenomenon is called optical feedback, a feature that is exploited in the high-power pumping of fiber lasers thereby, enabling broader applications (EL-DESSOUKY et al., 2014).

Interest in fiber lasers has been driven by the phenomenal growth in fiber-optic communications, which itself resulted from the fundamental breakthrough in producing silica optical fibers with extremely low light transmission losses (HECHT, 2015). One clear argument for the development of fiber laser technology has been its ready compatibility with optical fiber systems. This has been borne out by the successful integration of erbium-doped fiber amplifier (EDFA) technology into long-distance communications systems only a few years after initial laboratory demonstrations (NAKAZAWA; KIMURA; SUZUKI, 1989).

Prior to the invention of the EDFA, optical transmission systems had operated over long distances by the use of electro-optic regeneration (MEARS, 1999). As an optical pulse travels it is subject to all fiber losses and the information contained in the pulse will be lost, so that it does not happen, the signal can be boosted. Initially, the only viable method of doing this was to detect the incoming signal with a photodiode, convert it to an electronic signal, and amplify it, then use that signal to switch a laser and then convert it to an optical signal again, thus sending out a new optical pulse along the next length of the fiber. This type of system had the limitation of only being able to work with one wavelength and the system had to be designed to operate at a specific bit rate. In contrast, the EDFA offers direct amplification independent of the signal bit rate and has the ability to allow greater distance between amplification. Also, it is a simpler device when compared to regenerative systems, and could simultaneously amplify signals at two or more different wavelengths, can be combined with wave division multiplexing (WDM) technology and benefiting the

dense wave division multiplexing (DWDM) in present communication systems (KEISER, 1999).

The EDFA was first demonstrated by Professor David N Payne and his team at Southampton University (UK) in 1986 (PAYNE et al., 1987). They can efficiently amplify light in the C band and L band, where the losses of telecom optical fibers become the lowest in the entire optical communication bands. For a typical setup of EDFA, a core of a fiber is doped with a percentual piece of rare-earth, erbium (Er^{3+}), changing the reflexive index, that can provide laser amplification via stimulated emission when it is optically pumped with other light injected into the fiber (DESURVIRE; ZERVAS, 1995). Figure 8 illustrates a typical setup of EDFA and an energy diagram of erbium in 1480 nm, showing how amplification takes place at 1550 nm.

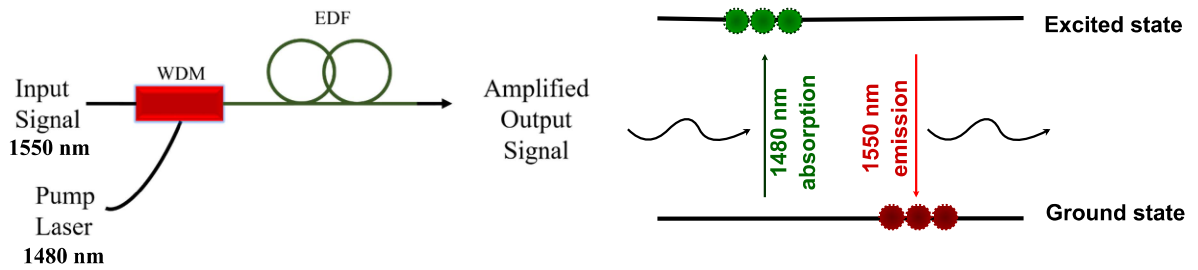


Figure 8 – Schematic setup of a simple erbium-doped fiber amplifier and energy diagram of erbium in 1480 nm.

In the shown case, the active fiber is pumped with light from two laser sources. For the pump light, there are two typical wavelengths to pump an EDFA, 980 or 1480 nm, because of the interaction of the Er^{3+} ions. The light for amplification is most often present in a wavelength around 1550 nm. Both power sources are coupled and launched into the optical doped fiber by a WDM. When an EDFA is pumped at 1480 nm, Er^{3+} ion doped in the fiber absorbs the pump light and moves out for the excited state, when sufficient power is present in the fiber and most of the electrons are in the upper level the population inversion is created and the amplification occurs by a stimulated emission, that emits photons around 1550 nm, the same wavelength than initial laser. The electrons that went to the ground state are excited again e back to an excited state, this process continues until the pump power is not capable more interacting with the electrons. The capacity of amplification is directly relational with the fiber doped characteristics. The process is same for 980 nm.

However, the vantage fiber offers over a conventional laser medium is the decoupling of the relationship between the length of the gain medium and the pump beam focusing. The confinement of the light power within the fiber core ensures that pump intensity is maintained along with the fiber for a hundred of thousands of kilometers, just subject

to losses through absorption or scattering, as seen before. The small core diameter of single-mode fibers also ensures that the power density is very high. These factors enable full operation lasing and becomes a differential whereas conventional solid-state analog, where pumping of very weak absorption when replicated in a long length of fibers (QUIMBY, 2006). Lasers have most diverse applications, such as in cosmetics treatments for acne and hair removal (LIEW, 2002), surgeries for cancer diagnosis and therapy and eye lens correction (DONALDSON et al., 2013), industrials for cutting and heat of components (WANG*; XIE, 2005), military, science and technology (KAUSHAL; KADDOUM, 2017), and communications systems for optical fiber communications, underwater communication networks and space communication, radars and satellites (ARNON; KOPEIKA, 1997). All these applications are employed the most diverse techniques such as ultrashort pulsed lasers, doped-lasers, random lasers, femtosecond lasers, multi-wavelength fiber lasers, and many others (SILFVAST, 2004).

1.2.1 Multi-wavelength fiber laser

The development of multi-wavelength laser sources has grown exponentially in recent years. Part of this rapid progress has taken place due to their potential applications such as in coherent light source for wavelength division multiplexing (WDM) schemes (KEMAL et al., 2016; AGRELL et al., 2016; ZHONG et al., 2018). WDM is a fiber-optic transmission technique that enables the use of multiple light wavelengths to send data over the same medium. These laser source technologies also have other applications, such as in fiber sensors (HAN et al., 2005), gas spectroscopy (MARSHALL; STEWART; WHITENETT, 2006), phased array antennas (JEON; LEE, 2014), and microwave generation (FU et al., 2010). Among other features, multi-wavelength fiber laser sources are largely exploited mostly due to their high long-term stability (FENG et al., 2019), large signal-to-noise ratios (ZHANG et al., 2017), and flexible wavelength tuning abilities (HE et al., 2018; LI et al., 2018).

Such laser sources can be fully made in all-fiber configurations allowing not only mechanically robust and compact structures, but also low levels of intracavity losses. Some examples of multi-wavelength fiber laser architectures can be constructed by using nonlinear optical loop mirrors (LIAN et al., 2019), fiber Bragg gratings (YAO et al., 2018), Mach-Zehnder interferometers (BIANCHETTI et al., 2018), Fabry–Perot filters (PAN; LOU; GAO, 2006), Sagnac fiber loop filters (MOON et al., 2007), Lyot filters (ZHAO et al., 2018), and also nonlinear effects such as nonlinear polarization rotation effect (FENG; TAM; WAI, 2006b), four-wave mixing (AL-ALIMI et al., 2018), and stimulated Brillouin scattering (SBS) (MAMDOOHI et al., 2018).

Specifically, multi-wavelength Brillouin fiber lasers (MBFLs) have attracted much attention due to their promising features, such as good stability at room temperature

(LIU; WANG; DONG, 2008), tunable narrow-linewidth frequency scheme (GALINDO-SANTOS et al., 2016; WANG et al., 2016), low-intensity noise (SHIRAZI et al., 2008), and a broad tunable range (NASIR et al., 2008). On the other hand, a current bottleneck of MBFLs is its narrow frequency shift that becomes a challenge for the de-multiplexing and signals filtering process for optical communication operations (WANG et al., 2013b; AL-ALIMI et al., 2017). In this perspective, several different schemes have been developed to further expand the MBFLs frequency spacing up to 20 GHz range, such as figure-of-eight configuration (PARVIZI et al., 2011), micro-air gap cavity (TIU et al., 2016), and four-port circulator (SHEE et al., 2011). Other approaches that support this development are by employing two metal-coated fiber planar mirrors and a Sagnac reflector (OH et al., 2002), as well as toggling an optical switch (ZHOU et al., 2016). Although these configurations enable the generation of MBFLs with different Brillouin frequency spacings, in most cases, these configurations are complex, requiring sophisticated amplification schemes with long fiber spools and high BP powers.

1.2.2 Nonlinear Fiber Laser

The nonlinear effects, are phenomena that modify the optical properties of a material system by the presence of light. For the generation of the nonlinear effects to be possible, is necessary to insert into the medium an intense light, and lasers can be used for the generation of light with high optical intensities (BOYD, 2020). Equation 1.4 represents the polarization response of material on the electric field E , we can write it as Taylor expansion

$$P = \sum_i P^{(i)} = \varepsilon_0 \chi^{(1)} E + \varepsilon_0 \chi^{(2)} E^2 + \varepsilon_0 \chi^{(3)} E^3 + \dots, \quad (1.4)$$

where $\chi^{(1)}$ is the linear susceptibility and the nonlinear contributions are represented by the nonlinear susceptibilities $\chi^{(i)}$ ($i \geq 2$) of order i . Second and third-order effects are also called quadratic and cubic order.

In most cases, one exploits either the quadratic nonlinearity or the cubic nonlinearity of the medium. The most important effects are parametric nonlinearities and delayed nonlinear response. Parametric nonlinearities occur in materials with $\chi^{(2)}$ nonlinearity and give rise to effects such as frequency doubling, sum and difference frequency generation, and parametric amplification. Also parametric nonlinearities, but arising from the $\chi^{(3)}$ nonlinearity, the Kerr effect, in general, modifies the refractive index and is related to effects like self-focusing, self-phase modulation, cross-phase modulation, four-wave mixing, and modulational instability. Effects of the delayed nonlinear response result from the nonlinear polarization proportional to the third power of the electric field strength, are

spontaneous and stimulated Raman scattering, an interaction of light with optical phonons, and Brillouin scattering, an interaction with acoustic phonons (BOYD, 2020).

Optical phonons involve the oscillation of neighbored ions with a phase difference of around 180° . They have much higher frequencies in the terahertz region and are related to Raman scattering. Acoustic phonons are related to long-wavelength vibrations, where neighbored ions oscillate nearly in phase. They have relatively low frequencies in the gigahertz region and are related to Brillouin scattering.

In optical fibers, the high intensity resulting from a small mode area becomes the nonlinearities most strong and easy to be generate. Silica has a relatively weak nonlinear coefficient, and initially, these effects acted only as essential nonlinearities for achieving certain functions, e.g. pulse compression, or they constituted limiting effects in high-power fiber lasers and amplifiers (BERGER, 1977). Currently, there are already developed techniques for increasing the nonlinearity present in optical fiber, modifying the refractive index during manufacturing adding elements such as a germanium GeO_2 . The new doped fiber is called a highly non-linear fiber (HNLF) and is used in diverse applications areas such as nonlinear pulse compression (SCHULTE et al., 2016), supercontinuum generation (YEOM et al., 2008), parametric fiber devices (FOTIOU; PARRILO; MORARI, 2005), Raman lasers (ASTAPOVICH et al., 2018), fiber-optic sensors (HAN; WU; LU, 2021), and communication systems (BAHRAMI et al., 2018).

1.3 Objectives

This dissertation proposes and experimentally demonstrate a generation of a multi-wavelength Brillouin-Erbium fiber laser in multiple frequency spacing configurations. By employing a laser source of narrow linewidth (1kHz), 25 km of a non-zero dispersion-shifted fiber (NZDSF) as the Brillouin gain medium, and a compact all-fiber setup with low loss, single, double, and triple frequency spacing configurations are obtained with BP as low as 1 mW.

The specific objectives of this work are listed as follow:

1. To develop and evaluate experimental configurations and select for testing setups.
2. To develop and to apply a setup for a Brillouin amplification
3. To develop a Brillouin laser with different types of fibers
4. To test different pump powers for characterization of non-linear effect Brillouin in different setups
5. To develop a multiples wavelength Brillouin fiber laser and test different setups.

1.4 Contributions

The publications resulting from this dissertassion are listed bellow:

1. **Pedruzzi, E.**, Silva, L. C., Leal-Junior, A. G., Castellani, C. E. (2022). Generation of a multi-wavelength Brillouin erbium fiber laser with low threshold in multiple frequency spacing configurations. *Optical Fiber Technology*, 69, 102832.
2. **da Silva, E. P.**, Pereira, K., Martins, G. R., Junior, V. N., dos Reis, L. B., Castellani, C. E. S. (2019, November). Low Threshold and Highly Efficient All Fiber Brillouin Laser. In 2019 SBMO/IEEE MTT-S International Microwave and Optoelectronics Conference (IMOC) (pp. 1-3). IEEE.
3. Silva, L. C., **Silva, E. P.**, Audibert, F. R., Castellani, C. E. (2020). Simulation solution for single and cascaded multi-wavelength Brillouin fiber lasers based on an analytical model. *Optical Fiber Technology*, 59, 102317.
4. Rebuli, G. S., Silva, L. C., **Pedruzzi, E.**, Leal-Junior, A. G., Segatto, M. E., Castellani, C. E. Spectral Optimization of Stokes Channels for Multi-Wavelength Brillouin Fiber Lasers. Submitted to *Laser Physics*.

1.5 Dissertation Structure

This dissertation is organized as follows: the overview of optical fiber and optical fiber laser is presented on Chapter 1. In addition, in Chapter 2, are introducing the Stimulated Brillouin Scattering effect and your peculiarities being a non-linear effect. The development of a Brillouin laser and testing of the three setups with multiples frequency spacing are presenting in Chapter 3 and 4, respectively, offer the results for each of them. At the end, we present the conclusions gained from the work, as well as future work for improvements and continuation of the study.

2 Brillouin Scattering

In 1920, Leon Brillouin discovered a new kind of light scattering, Brillouin scattering, which occurs as a result of the interaction of light with a transparent material's temporal periodic variations in density and refractive index. Many advances have since been made in the study of Brillouin scattering, in particular in the field of fiber optics. The physics behind Brillouin scattering can be understood as an inelastic effect in which part of the incident beam energy is absorbed and maintained in the medium in the form of structural vibrations, causing the light to be scattered back with less energy, or in a lower frequency, than previously (HECHT, 2004). Due to its robustness, low threshold power, narrow spectrum and simplicity of operation, stimulated Brillouin scattering (SBS) has become attractive for both sensing and telecommunication applications.

The present chapter is dedicated to the study of the principles of stimulated Brillouin scattering (SBS). Section 2.1 explains the mechanism of light scattering in different media, while sections 2.2 and 2.3 apply these concepts to particular cases of Brillouin scattering. Section 2.2 provides an overview of spontaneous Brillouin scattering while section 2.3 describes in detail the case of stimulated Brillouin scattering.

2.1 Light scattering

A solid is formed by a large number of particles linked by cohesion forces, which makes particle movement restricted. Each atom moves only within a small neighborhood performing a vibratory movement around its equilibrium point. This vibratory movement is characterized by the presence of the restoration force that acts to restore the balance between the particles and the medium. This vibration around the balance position is known as small oscillations (LANDAU; LIFSHITZ, 2013).

Light scattering is a consequence of the presence of particles in the optical path of light. The presence or not of inhomogeneities in this medium alters the characteristics of the propagation of scattered light. In general, the variation in polarization is a consequence of fluctuations in the density of dipole moments, N , and in polarizability, α_p . The first fluctuation is associated with acoustic modes and the second is due to optical modes (JR; FRAGNITO, 2006). Manipulating the Equation 1.4 in function of fluctuations associate and in relation to time, have:

$$\begin{aligned}
\ddot{P} = & N_0 \alpha_{0p} E_0 \omega_0^2 e^{-i\omega_0 t} + \\
& \delta N \alpha_{0p} E_0 (\omega_0 \pm \omega_{ac})^2 e^{-i(\omega_0 \pm \omega_{ac})t} + \\
& N_0 \delta_0 (\omega_0 \pm \omega_{opt})^2 e^{-i(\omega_0 \pm \omega_{opt})t}
\end{aligned} \tag{2.1}$$

The first term of the Equation 2.1 represents Rayleigh backscattering. This process depends on the initial amplitude of the quantities involved and does not change the optical properties of the medium. It is generated from stationary inhomogeneities, such as structural and topological defects. The atoms present in the dielectric medium are in constant vibration, this vibrational state can be divided into two groups, acoustic vibration mode and optical vibration mode. The second term of the equation represents the acoustic vibrational mode and the third term represents the optical vibrational mode. In acoustic vibration mode, the particles move in phase, so the polarizability is constant. In this case, the variation in polarization stems from the fluctuation in the density of dipole moments, δN . The radiation generated by this component is responsible for the Brillouin backscattering bands. In optical vibration mode, the particles vibrate out of phase, generating fluctuations in polarizability. The radiation generated by this fluctuation is responsible for the Raman backscattering bands (AGRAWAL, 2000). The presence the signals positive and negative denote the existence a higher frequency than the incident light, called the anti-Stokes wave, and a component having a lower frequency than the incident light, called the Stokes wave. Schemes of Rayleigh, Brillouin, and Raman peaks in optical fiber are shown in Figure 9.

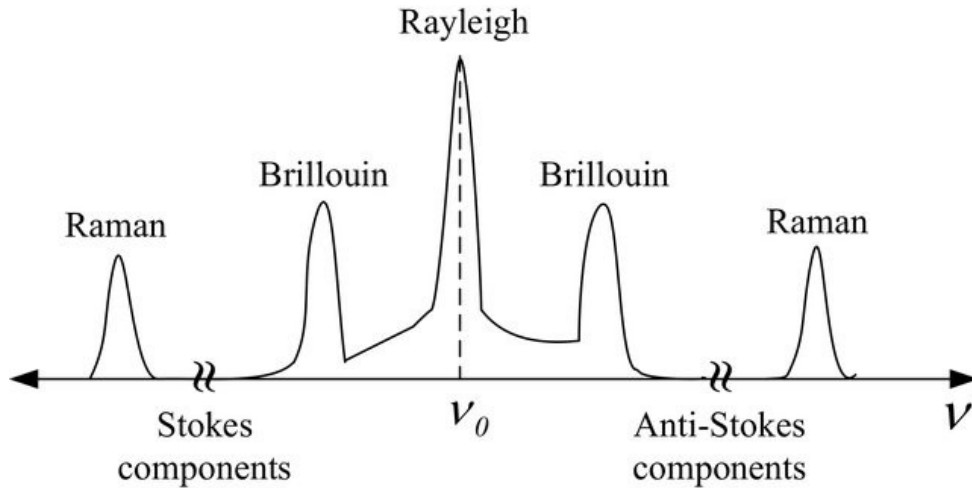


Figure 9 – Schematic of Rayleigh, Brillouin, and Raman peaks in optical fiber (YÜCEL et al., 2017).

where ν is the frequency axis.

It is composed of five bands, the central band is the Rayleigh scattering, which is the strongest. The two closer peaks of the central band are referents of the Brillouin

scattering. The peaks furthest from the central band are related to the Raman scattering. The process of the Brillouin and Raman scattering are depended on the dynamic of the medium while the Rayleigh scattering is related to the stationary inhomogeneities. Depending on the intensity of the incident light, we may get either spontaneous scattering for low intensities of the incident light, or stimulated scattering for high intensities of incident light (BOYD, 2020).

Brillouin scattering arises from the interaction of light with propagating density waves, caused by the part of the third-order nonlinearity of the medium related to acoustic phonons. Brillouin scattering may occur spontaneously when pump light scatters off the particles that are present in thermal equilibrium. Due to the Doppler effect, the frequency of the scattered light is downshifted from the frequency of the incident light. Because of this difference, the incident and scattered waves follow together, causing variations in the density of the media, which in turn causes refractive index variations. In optical fibers, the incident light scatters off the refractive index variations in the direction opposite to the direction of propagation of the pump light, thus giving rise to the Brillouin scattering phenomenon (BOYD, 2020).

Brillouin Scattering may also be stimulated. As mentioned above, for intense beams such as laser light, traveling in a medium such as an optical fiber, the interaction between an intense pump light and acoustic waves, generates the SBS. The phenomenon responsible is known as electrostriction, which is the tendency of materials to deformed in regions of high optical intensity. Electrostriction creates a dynamic acoustic grating, which in turn causes variations in the refractive index of the material. As a result, laser light may undergo stimulated Brillouin scattering due to the variations in the medium. SBS is frequently encountered when narrow-band optical signals are amplified in a fiber amplifier. In fact, SBS introduces the most stringent power limit, commonly referred to as the Brillouin threshold, for the amplification or even passive propagation of narrow-band optical signals, such as those used in telecommunications (BOYD, 2020).

2.2 Spontaneous Brillouin scattering

Equation 2.2 is associated with the presence of fluctuations in the material medium, it represents the wave scattered by the fluctuations present in the medium, or in the optical path (BOYD, 2020).

$$\nabla^2 \mathbf{E} - \frac{n^2}{c^2} \frac{\partial^2 \mathbf{E}}{\partial t^2} = \mu_0 \frac{\partial^2 \mathbf{P}_{\text{ind}}}{\partial t^2} = \mu_0 \frac{\partial^2 (\Delta \epsilon \mathbf{E})}{\partial t^2} \quad (2.2)$$

It is important to develop a macroscopic description of the light scattering process, whereby the light scattering process occurs as a result of fluctuations in material density and temperature. In general, the dielectric constant can be written in terms of density and

temperature, however, the contribution of temperature in this process is approximately 2% (BOYD, 2020). Thus, in terms of thermodynamic variables, it is defined as:

$$\Delta_\epsilon = \left(\frac{\partial \epsilon}{\partial \rho} \right)_T \Delta \rho, \quad (2.3)$$

where

$$\left(\frac{\partial \epsilon}{\partial \rho} \right)_T = \gamma_e \rho_0, \quad (2.4)$$

where γ_e is the electrostrictive constant of the material. The fluctuation in density, Δ_ρ , can be written in terms of pressure p and entropy s (BOYD, 2020), as:

$$\Delta_\rho = \left(\frac{\partial \rho}{\partial p} \right)_s \Delta p + \left(\frac{\partial \rho}{\partial s} \right)_p \Delta s \quad (2.5)$$

The first term describes adiabatic fluctuations and the second term represents isobaric fluctuations in density. The equation shows that the terms have different natures. The first term is related to pressure variation, therefore it is related to dynamic processes such as acoustic phonons. This component leads to the Brillouin scattering study. The second term refers to entropy variation, therefore, it is related to point defects, and the topological and structural disorders present in the medium. This term refers to the process of Rayleigh scattering.

Considering $\Delta_s=0$, i.e. constant entropy, the fluctuation in density can be written as:

$$\Delta_\rho = \left(\frac{\partial \rho}{\partial p} \right)_s \Delta p \quad (2.6)$$

The fluctuation in pressure is a solution of the wave equation (BOYD, 2020) given by

$$\frac{\partial^2 \Delta p}{\partial t^2} - \Gamma \nabla^2 \frac{\partial \Delta p}{\partial t} - v_a^2 \nabla^2 \Delta p = 0 \quad (2.7)$$

$$v_a = \sqrt{\frac{1}{C_s \rho}} \quad (2.8)$$

The solution of this equation is:

$$\Delta p = \delta p_0 \exp[i(\mathbf{q} \cdot \mathbf{r} - \omega_{ac} t)] + c.c.. \quad (2.9)$$

This equation represents the pressure fluctuation in the medium, caused by an acoustic wave propagating in this medium. This disturbance propagates in the direction \mathbf{q} with frequency ω_{ac} .

The characteristic wavelengths of acoustic waves in silica are large compared to the dimensions of the molecules influenced by it. In this way, when an acoustic disturbance passes through a certain region of the medium, it displaces a large number of particles. This displacement, which occurs in the \mathbf{q} direction, has a collective characteristic, that is, many particles move in the same direction, as they are under the same perturbation. This collectivity feature is also called nonlocality, and the events associated with the acoustic wave are also nonlocal. As mentioned, acoustic phonons have the same frequency as the acoustic wave present in the medium, so the effects involved with these phonons are non-local. The idea of non-locality is related to the large number of particles that are influenced by the acoustic disturbance (ERINGEN, 1980).

Considering that the incident light is monochromatic, that is, it has a single optical frequency, inserting Equation 2.9 into Equation 2.6, the density is obtained in terms of pressure fluctuation. Taking this result into Equation 2.3, the dielectric constant in terms of the pressure fluctuation wave is obtained. Finally, substituting this result in Equation 2.2, which represents the scattered electromagnetic wave, it is obtained:

$$\nabla^2 \mathbf{E} - \frac{n^2}{c^2} \frac{\partial^2 \mathbf{E}}{\partial t^2} = \mathbf{F}_s + \mathbf{F}_{as} + c.c., \quad (2.10)$$

$$\mathbf{F}_s = \frac{\gamma_e C_s}{2} \Delta p_0 E_{L0} [(\omega_L - \omega_{ac})^2 \exp[i(\mathbf{K}_L - \mathbf{q}) \cdot \mathbf{r} - i(\omega_L - \omega_{ac})t]], \quad (2.11)$$

$$\mathbf{F}_{as} = \frac{\gamma_e C_s}{2} \Delta p_0 E_{L0} [(\omega_L + \omega_{ac})^2 \exp[i(\mathbf{K}_L + \mathbf{q}) \cdot \mathbf{r} - i(\omega_L + \omega_{ac})t]]. \quad (2.12)$$

The solution of Equation 2.10 represents the optical wave scattered by the fluctuation in the dielectric constant due to the pressure fluctuation. As represented in Equation 2.7, there is no external source generating the fluctuation in pressure. This fact characterizes the process as being spontaneous. The presence of the two frequency components indicates that the frequency of scattered radiation is different from the frequency of incident radiation, therefore, that the process is inelastic. The energy associated with this frequency is the thermal (acoustic) phonon energy. The optical frequency defined in Equation 2.13 is called the Brillouin Stokes frequency, and the frequency defined in Equation 2.14 is called the Brillouin anti-Stokes frequency.

$$\omega_L - \omega_{ac} = \omega_S \quad (2.13)$$

$$\omega_L + \omega_{ac} = \omega_{AS} \quad (2.14)$$

2.2.1 Brillouin frequency shift

Vibration modes are stationary or non-propagating vibrations. Its constant movement disturbs the surroundings, generating a disturbance in the distribution of pressure, density and the position of the particles. This disturbance propagates in all directions of the medium. In the case of optical fiber, the perturbation in the longitudinal direction is the most efficient in the light coupling process. The disturbance propagating in the direction transverse to the longitudinal axis of the optical fiber can be neglected (JR; FRAGNITO, 2006). This disturbance propagated as an acoustic wave, with wave vector \mathbf{q} and frequency ω_{ac} (BOYD, 2020). The consequence of the propagating disturbance is the generation of compression and rarefaction regions in the medium, which act as a mirror. Classically, it is this Bragg grating like structure that scatters the incident light.

The Brillouin Stokes frequency, Equation 2.13, is generated by the particles that are scattered, by the pressure wave, in the same direction and phase as the incident optical light, whereas the anti-Stokes Brillouin frequency, Equation 2.14, is generated by the particles that are displaced, by the pressure wave, in the same phase and opposite direction as the incident optical wave. As the frequency of the acoustic wave is the same for both situations, the spectrum of spontaneous Brillouin scattering is formed by two frequencies that are symmetrical with respect to the frequency of the incident optical field. The distance, in frequency, between the frequency of the incident optical wave and the frequency of the Brillouin Stokes or anti-Stokes wave is called the Brillouin frequency shift (BOYD, 2020).

$$\omega_{ac} = 2n\omega_0 \frac{v_a}{c} \sin(\theta/2) \quad (2.15)$$

Equation 2.15 shows that the Brillouin frequency shift, for a medium with refractive index n and whose pumping frequency is fixed, depends on the velocity of the acoustic wave and the scattering angle. Accounting for the definition of acoustic wave velocity given by Equation 2.8, any variation in the density of the medium generates variation in the velocity of the acoustic wave and, consequently, promotes variation in the Brillouin shift. This feature is very important because it leads to the use of Brillouin scattering as a sensing effect for disturbances that generate variations in the density of the medium, such as mechanical deformation and temperature (JR; FRAGNITO, 2006). Another important consideration of this equation concerns angular dependence. The Brillouin displacement is minimum for angles around $\theta = 0^\circ$, and maximum for angles around $\theta=180^\circ$. In the case

of optical fiber, the scattering that propagates is 180° with respect to the incident wave so the Brillouin displacement is:

$$\omega_{ac,max} = \Delta\nu_{Bmax} = 2n_{ir} \frac{\omega_0 v_a}{c} \quad (2.16)$$

The Brillouin Stokes backscattering process can be considered as a process of annihilation of an incident photon, followed by the creation of a phonon and a photon with a frequency lower than the frequency of the incident photon. On the other hand, the anti-Stokes Brillouin scattering process is considered as an annihilation process of an incident photon and a phonon present in the medium, followed by the emission of a photon with a frequency greater than the frequency of the incident photon. Thus, Brillouin Stokes backscatter is a phonon creation process and anti-Stokes Brillouin backscatter is a phonon annihilation process (AGRAWAL, 2000). Thus, the amplification of the acoustic wave represents an amplification of the Brillouin Stokes component, as it is associated with the creation of phonon.

Once the Brillouin frequency shift is known, the wavelength of the acoustic wave can be calculated as a function of this quantity. For this, consider that

$$v_a = \lambda_a \omega_{ac} = \lambda_a \Delta\nu_{Bmax} \quad (2.17)$$

$$\lambda_a = \frac{v_a}{\Delta\nu_{Bmax}}, \quad (2.18)$$

which represents the spatial periodicity of the wave that participates in spontaneous Brillouin scattering.

Although it has been considered that the scattered optical wave is monochromatic, this is not quite true, it has a line width that is proportional to the lifetime of the phonon involved in the process. Then, the Brillouin scattering linewidth, defined as the inverse of the phonon lifetime, is $\tau=1/|q|^2\gamma$, where Γ is the phonon decay rate (BOYD, 2020) given by:

$$\delta\omega = \frac{1}{\tau_a c} = |q|^2 \Gamma = 4\Gamma \frac{n^2 \omega_L^2}{c^2} \sin^2 \left(\frac{\theta}{2} \right). \quad (2.19)$$

2.3 Stimulated Brillouin scattering

It was shown in the previous section, then, that scattering results from fluctuations in the optical properties of the medium. Now the scattering process is evaluated when fluctuations are excited, therefore they are stimulated, with regard to electrostriction.

2.3.1 Electrostriction

Electrostriction is defined as the tendency of certain materials to deform in the presence of an electric field. This effect works as a coupling mechanism between acoustic and optical waves. It is a consequence of the increase in the internal energy of a medium (BOYD, 2020). This effect leads to stimulated Brillouin scattering.

We can explain the origin of this effect by observing the change in elastic potential energy per unit volume of a material immersed in an electric field of magnitude $|E|$. The presence of the electric field in a molecule induces a dipole moment given by $\mathbf{p} = \epsilon_0 \alpha \mathbf{E}$. The energy in the polarized molecule is:

$$U = -\frac{1}{2} \epsilon_0 \alpha E^2 \quad (2.20)$$

Assuming that the system is conservative and the electric field is non-oscillating, the force acting on the molecule is given by:

$$\mathbf{F} = \frac{1}{2} \epsilon_0 \alpha \nabla(E^2) \quad (2.21)$$

The positive sign indicates that the molecule is pushed to the region where the electric field gradient increases. With this result, it is possible to calculate the fluctuation in density due to the action of this force.

$$\Delta u = \frac{1}{2} \epsilon_0 E^2 \left(\frac{\partial \epsilon}{\partial \rho} \right) \Delta \rho \quad (2.22)$$

According to the first law of thermodynamics, this change in energy is equal to the work done to deform the medium (BOYD, 2020). So,

$$\Delta w = -p_s t \frac{\Delta \rho}{\rho} \quad (2.23)$$

In Equation 2.23, $p_s t$ represents the contribution of the electric field in the deformation process of the material medium. Equating $\Delta u = \Delta w$, and solving for $p_s t$, it have:

$$p_s t = -\frac{1}{2} \epsilon_0 \gamma_e E^2 \quad (2.24)$$

where $\gamma_e = \rho(\partial \epsilon / \partial \rho)$ is known as the electrostrictive constant. Two features should be highlighted in Equation 2.24. First, the negative sign shows that the electric pressure is negative in the region where the electric field acts. Second, that the electrostrictive pressure varies linearly with the amplitude of the electric field in the region. These two

characteristics of the electric field show that the increase in the electric field decreases the electrostrictive pressure in the region where the electric field acts. Thus, the increase in the electric field intensity causes a variation in the density, which can be considered as

$$\Delta\rho = \frac{1}{2}\epsilon_0\rho C_s\gamma_e E^2 \quad (2.25)$$

Equation 2.25 represents the change in material density induced by the applied electric field. However, this motion requires a time interval that is large compared to the oscillation time of optical waves. The material is therefore unable to follow the E-field oscillation, but is sensitive to the mean value $\langle E \rangle$. Thus, this equation is valid for non-oscillating fields (BOYD, 2020). For oscillating electromagnetic fields, it must be rewritten in terms of the mean value. So,

$$\Delta\rho = \frac{1}{2}\epsilon_0\rho C_s\gamma_e \langle \mathbf{E} \cdot \mathbf{E} \rangle \quad (2.26)$$

With Equation 2.26, it can find the third-order susceptibility, which is responsible for the Brillouin scattering process. For this, it is enough to consider the change in the optical property occurring as a function of electrostriction. The variation on susceptibility is:

$$\Delta\chi = \frac{1}{2}\epsilon_0\rho C_s\gamma_e^2 \langle \mathbf{E} \cdot \mathbf{E} \rangle \quad (2.27)$$

This variation in density also changes the refractive index (BOYD, 2020), which can be calculated using the following equation:

$$\Delta n = \frac{n_0}{2\epsilon_0} C_s \gamma_e^2 \langle \mathbf{E} \cdot \mathbf{E} \rangle \quad (2.28)$$

The elasto-optic effect is a linear effect, thermal acoustic waves are present in the medium and cause a disturbance in the refractive index, scattering light. Electrostriction is a non-linear effect through which light excites acoustic waves. Basically, by this effect, an electric field causes tension in the material, whose amplitude is proportional to the square of the amplitude of the electric field associated with the resulting electromagnetic wave. The force that generates this tension is given by Equation 2.21.

The connection of this effect with stimulated Brillouin backscattering can be understood through the interaction between the spontaneously scattered optical fields and the incident optical field. Assume that, initially, a continuous laser is launched into the optical fiber. Being continuous, the optical intensity is uniform along the length of the fiber, promoting a zero gradient. However, the pumping laser is scattered by the Bragg grating, formed by the thermally excited acoustic waves, which is responsible for the spontaneous

scattering (AGRAWAL, 2000). Through this spontaneous scattering, two optical fields come to exist in the medium, therefore in the same region of space. As already mentioned, it is known that there is a difference in the frequency of the waves scattered by the thermal vibrations and the pumping wave. This generates an interaction between the optical fields, establishing an optical gradient between the maximum beat and minimum beat regions. In the region where the beating is maximum, the electric field of the optical wave is also maximum, acting on the charges in the medium and inducing a dipole moment transition, as well as a mechanical stress distribution. The latter, in turn, relaxes by emitting acoustic waves. This change in mechanical stress distribution due to the presence of the electric field is called electrostriction or electrostrictive effect. From this point, electrostriction generates the acoustic wave, which in turn scatters the incident optical field. As the velocity of the acoustic wave is different from the velocity of the pumping wave, the scattered wave has a frequency given by the Doppler effect, which is the same value found for spontaneous scattering (BOYD, 2020; AGRAWAL, 2000). This scattering process amplifies the beat between the optical waves, the consequence of which is the amplification of the acoustic wave, and thus a feedback mechanism is initiated.

In summary, the pumping wave is scattered, generating the Stokes wave, whose frequency is different, thus, a beat is established generating acoustic waves that, again, scatter the pumping wave, reinforcing the beat, and the cycle repeats. It can be said that electrostriction is an acoustic wave amplification mechanism, whose consequence is the transfer of energy from the pumping wave to the scattered wave.

2.3.2 Brillouin threshold

During spontaneous Brillouin scattering, the amplitude of the electric field associated with the electromagnetic wave was considered small enough not to significantly alter the properties of the thermally excited acoustic waves, the acoustic phonons. However, the scenario changes when the amplitude of the electric field associated with the incident electromagnetic wave is large enough to mechanically deform the medium. In this case, a second effect becomes important: electrostrictive, already there mentioned. The intensity of the incident optical field required to switch from the spontaneous Brillouin scattering regime to the stimulated Brillouin scattering regime is called the Brillouin threshold (BOYD, 2020).

In general, the efficiency in the generation of nonlinear optical effects results from a combination between the intensity of the incident optical field and the effective length of the interaction region. An incident optical field is understood to mean the electromagnetic field associated with the incident electromagnetic wave. In the free medium, the optical field strength is given by $P_{\text{bomb}}/\pi\omega_0^2$, although the pumping power is large, the interaction length is small. On the other hand, in optical fiber, ω_0 can be approximated for the core

diameter and the interaction length varies from a few centimeters to tens of kilometers. Thus, the intensity of the optical field easily reaches values sufficient to generate non-linear effects, such as the Brillouin and Raman scattering processes (AGRAWAL, 2000). The Brillouin threshold is given by:

$$P_{cr}^B \approx \frac{21A_{eff}}{\gamma_{pol}g_0L_{ef}} \quad (2.29)$$

where A_{eff} is the effective area of optical fiber. L_{ef} represents the effective length of the optical fiber, it tends to $1/\alpha$ for long-length optical fibers. α is a optical loss. γ_{pol} is the polarization factor, this means that if the electric field of the incident electromagnetic wave has the same polarization as the electric field of the electromagnetic wave generated in Brillouin scattering the polarization factor is 1, on the other hand if the polarizations are different this factor is 1/2. The first case occurs in polarized fibers, the second case occurs in non-polarized fibers.

2.3.3 Brillouin gain

Stimulated Brillouin scattering (SBS) is the most efficient nonlinear amplification mechanism in optical fibers, in which a large gain may be obtained under the pump power of several milliwatts (OLSSON; ZIEL, 1986). The Brillouin gain spectrum (BGS) is determined by measuring the amplification of the incident light when the frequency difference between the pump and the Brillouin peak corresponds to the Brillouin frequency shift. The Brillouin shift can be rewritten by:

$$\nu_B = \frac{2nV_a}{\lambda} \quad (2.30)$$

where V_a is the acoustic velocity within the fiber, n is the refractive index and λ is the wavelength of the incident lightwave. The Brillouin gain is given by:

$$g_B(\nu) = g_0 \frac{(\Delta\nu_{B/2})^2}{(\nu_B - \nu)^2 + (\Delta\nu_{B/2})^2} \quad (2.31)$$

where $\Delta\nu_B$ is the full-width at half maximum (FWHM). The BGS peaks at the Brillouin frequency shift ν_B , and the peak value is given by the Brillouin gain coefficient g_0

$$g_0 = \frac{2\pi n^7 p_{12}^2}{c\lambda_p^2 \rho_0 V_a \Delta\nu_B} \quad (2.32)$$

Equation 2.32 represents the maximum gain for Brillouin scattering, which occurs when $(\nu_B - \nu)$, that is, when the optical frequency of excitation is equal to the frequency of Brillouin Stokes scattering. Where p_{12} is the longitudinal elasto-optic coefficient, ρ_0 is

the density, λ_p is the pump wavelength and c is the vacuum velocity of light (HEIMAN; HAMILTON; HELLWARTH, 1979).

When the spectral linewidth of the pump $\Delta\nu$ becomes comparable with the spectral width of the Brillouin $\Delta\nu_B$, the Brillouin gain is reduced by a factor of $1 + \Delta\nu/\Delta\nu_B$, and this ensures that a narrow linewidth causes a low threshold. The Brillouin gain depends on the pump spectral linewidth, considerably influencing the performance of fiber amplifiers and lasers (SILVA; CASTELLANI, 2021), and can be described by:

$$\gamma = \left(\frac{g_B}{A_{eff}} \right) \times \left(\frac{1}{1 + (\Delta\nu/\Delta\nu_B)} \right) \quad (2.33)$$

In Equation 2.33 the behavior of the Brillouin gain as a function of the spectral width of the pump is presented. The Brillouin threshold equation can be rewritten in function as the peak γ as:

$$P_{cr}^B = \frac{\Lambda + \sqrt{\Lambda^2 + 4\Lambda}}{2\gamma L_{ef}} \quad (2.34)$$

where $\Lambda = -\ln(P_{sL}\gamma L)$, and P_{sL} is the input Stokes power (SILVA; CASTELLANI, 2021).

3 All fiber Brillouin Laser

SBS can convert nearly all of the useful signal waves into the backward propagating Stokes wave if the signal power and fiber length product are great enough. In this case, the SBS process fuels laser action at the frequency of the Stokes wave on account of feedback provided by the laser cavity. In fact, they allow a Stokes wave begins to dissipate, it can also serve to cascaded for new Stokes and phonon fields (JR; FRAGNITO, 2006).

This chapter focuses on the construction of a all fiber Brillouin laser in ring cavity, using a pumping laser with bandwidth of 1kHz and three different types of optical fibers: A 25 km Non-Zero Dispersion-Shifted Fiber (NZDSF), A 2 km Highly Non-linear Fiber (HNLF) and A 15 km Dispersion Compensating Fiber (DCF) in the configuration. Due to the combination of some of the characteristics of those fibers with the very low bandwidth of the pump source, it were able to find very low thresholds, maintaining a high efficiency, even when using only 2km of a fiber gain media. Moreover, here is discuss some of the laser characteristics, such as: efficiency, threshold, time and frequency stability, and Stokes shift, for variations of pump power and cavity output coupling ratio.

3.1 Experimental Setup

The experimental setup is shown in Figure 10 using a simple ring-cavity setup, which is pumped by a 1565 nm unpolarized laser (TeraXion-Pure Spectrum laser - Tunable Narrow Linewidth) with a maximum power of 14 mW, and bandwidth of 1kHz, used as a Brillouin pump (BP). The pump goes through a circulator used to ensure unidirectional propagation of the counter-propagating stokes wavelength inside the cavity, which is generated in the fiber under test (FUT). Three types of fibers were tested: the NZDSF and DCF in silica and the HNLF made of silica doped with 12% concentration of Germanium Oxide (GeO_2). The main properties of each fiber are summarized in Table 1, where A_{eff} is the optical mode effective area at 1550 nm, α is the optical loss at 1550 nm, L is the fiber length. In more efforts, the pump power was varied from 0 to its maximum value of 14 mW and various output couplers with output ratios varying from 10% to 90% were used. In the laser output was used an optical spectrum analyzer (OSA) (AP268-A/C - Appex technologies) with resolution of 1.12 pm. The splicing loss between the FUT and the other connections is about 0.1dB for all connectors.

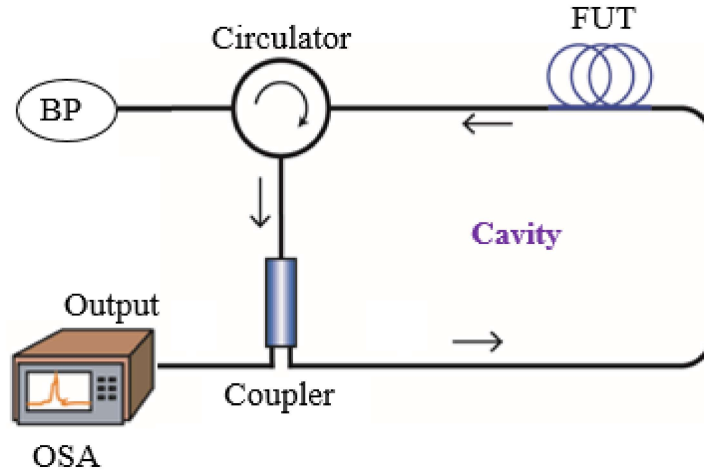


Figure 10 – Experimental laser setup: BP: Brillouin pump, FUT: fiber under test, OSA: Optical Spectrum Analyzer.

Table 1 – FUT properties

	NZDSF	HNLF	DCF
L (km)	25	2	15
α (dB/km)	0.201	0.300	0.265
A_{eff} (μm^2)	45.840	19.400	27.000
Peak Ramam Gain	-	2.5	-
Efficiency ($\text{W} \cdot \text{km}$) ⁻¹	-	-	-

3.2 Results and Discussions

3.2.1 Laser Output Power

The laser output power as a function of the pump power for all three FUT can be seen in Fig. 11. Here was chose the 90% output coupler ratio. In Fig. 11 it can be observed that highest output power achieved is around 7.278 mW obtained when using the NZDSF, which also presents the lower level of threshold and highest level of efficiency. This is mostly due to the fact that this fiber is 25 km long. Nevertheless, it is also important to note that the performance of laser using the HNLF is close to the NZDSF, but using only 2 km of fiber as the gain medium. This can be attributed to the fact that the HNLF used in this experiment has a much higher nonlinearity due to its reduced effective area and its doping with GeO_2 .

In order to analyze the power fluctuations at the laser output, power measurements were made every 1 minute for 35 minutes for each FUT for pump powers from 0 to 14 mW using a coupling ratio of 90 %. The maximum variation percentages for the lasers using NZDSF, HNLF and DCF were 6.7%, 8.8 % and 4.6%, respectively, which were obtained under a pump power of 14 mW and that can be seen in Fig. 12. These variations can be

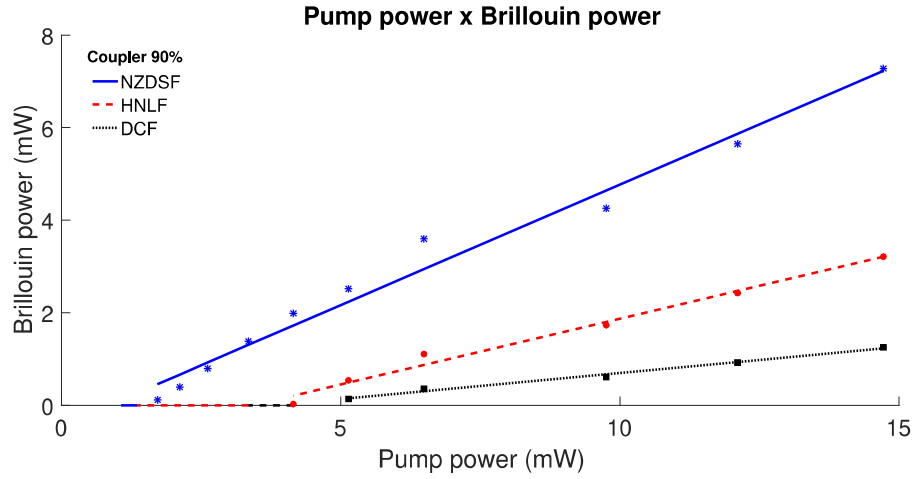


Figure 11 – Laser output power as a function of the pump power for a output coupling ratio of 90% for all three FUT.

attributed mostly to fluctuations of the pump source that were measured under the same circumstances to be at maximum around 7.7%, which is also shown in Fig. 12.

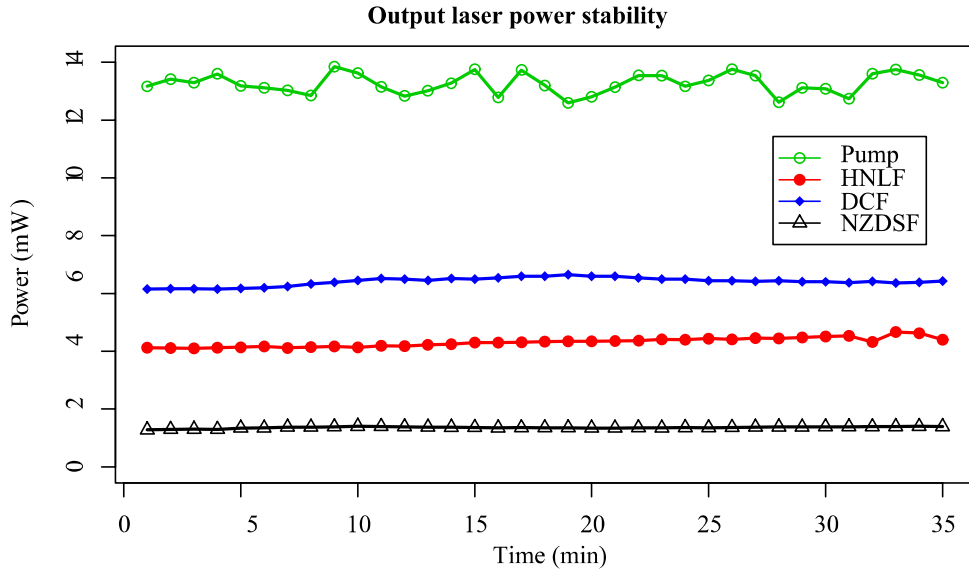


Figure 12 – Output laser stability analysis for a coupling ratio of 90 % and under a pump power of 14 mW.

3.2.2 Threshold and Efficiency

Fig. 13 shows the variation of the threshold for different percentages of output coupling ratio. Note that the threshold increases with the percentage of the coupler, since less power is recirculated inside the cavity. For the output coupling of 10%, as expected, was observed the lowest threshold for all FUT. For the NZDSF was found the lowest

threshold power at 1.148 mW, while with the HNLF the threshold power found was 1.718 mW and 4.15 mW when using the DCF.

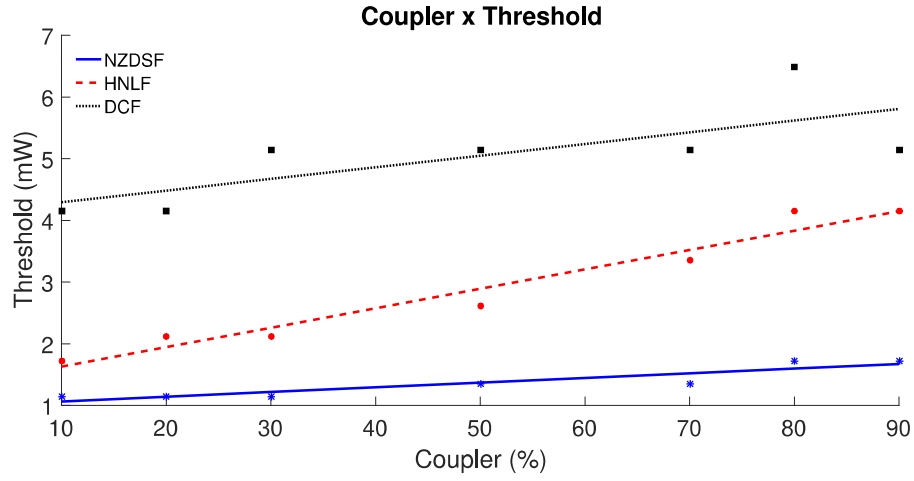


Figure 13 – Threshold as a function of the output coupling ratio for tests using all three FUT.

The laser efficiency was evaluated again for variations of the output coupler for all three FUT, which can be seen in Fig. 14. The efficiency also increases when increasing the percentage of the output coupler. This is expected, since a higher coupling ratio means that more power is being extracted from the cavity. The highest efficiency of 49.43% was obtained when using the NZDSF and a 90% output coupler. These values were 28.05% for the HNLF and 6.427% for the laser using the DCF. Again, it is important to highlight the fact that even using modest pump powers, it were able to achieve good values for the pump-stokes conversion using a simple laser configuration. Moreover, it is also important to note that the combination of the high non-linearity found in our HNLF with our pump source of narrow bandwidth allowed the demonstration of a Brillouin fiber laser of low threshold (4.15 mW) and high efficiency (28.05%) for a fiber with only 2 km.

3.2.3 Brillouin spectrum

The laser output was analyzed by an OSA for all the three FUT and the spectra obtained can be seen in Fig. 15. The high resolution of 1.12 pm of the OSA allows to see the difference in the Brillouin shifts obtained when using different fibers. The stokes wavelengths are shifted from the pump by 10.575 GHz for the NZDSF, 9.96 GHz for the HNLF and 11 GHz for the DCF. The shifts found when using the NZDSF and the DCF are similar since those fibers are made mostly of pure silica, with only a small percentage of dopants. This is different for the laser using the HNLF which has a doping concentration of GeO₂ estimated around 12%. The smaller value of 9.96 GHz separation obtained when using this fiber is expected since GeO₂ is known to present a smaller Brillouin frequency shift when comparing to silica.

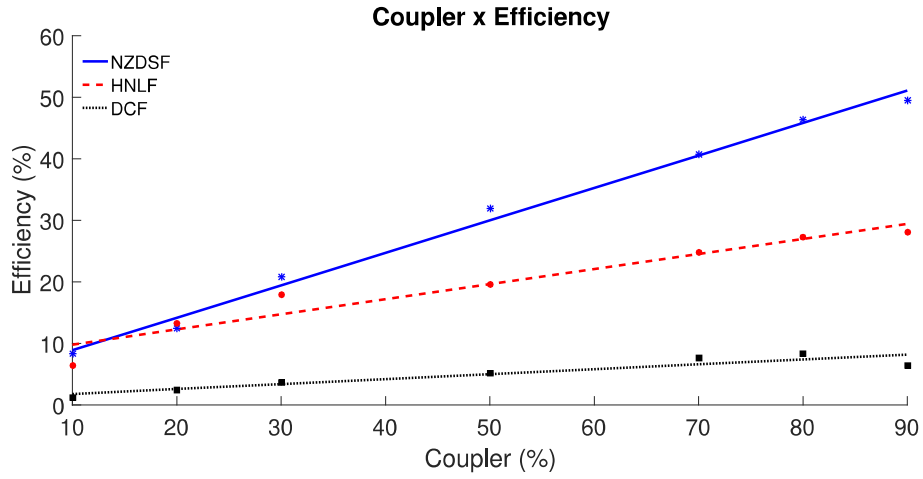


Figure 14 – Efficiency as a function of the output coupling ratio for tests using all three FUT.

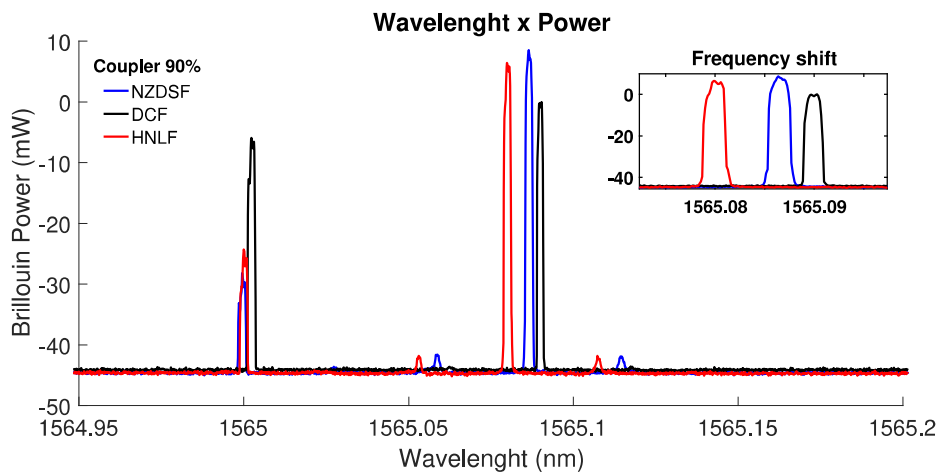


Figure 15 – Optical spectra at the laser output for all three FUT used as the gain media.

4 Multi-wavelength Brillouin fiber lasers

From the characterization made in Chapter 3, it was possible to choose the best fiber as a Brillouin gain medium. The NZDSF presented threshold as low as 1.15 mW and efficiencies as high as 49.43% and allow can potentially be adapted for cascade laser.

The generation of the cascaded multi-wavelength Brillouin erbium fiber laser (MWBEFL) with a low threshold is presented in this chapter. By employing a laser source of narrow linewidth (1 kHz), 25 km of a non-zero dispersion-shifted fiber (NZDSF) as the Brillouin gain medium, and a compact all-fiber setup with low loss, single, double, and triple frequency spacing configurations are obtained with BP as low as 1 mW.

4.1 Experimental setup

The configuration of the proposed multi-wavelength Brillouin erbium fiber laser (MWBEFL) with single frequency spacing is showed in Figure 16. In this configuration, the BP power is a laser at 1565 nm (teraXion-pure spectrum laser-tunable narrow linewidth) with a maximum power of 14 mW, and a bandwidth of 1 kHz. In this scheme, the BP is amplified by an EDFA that acts as a gain block, which is composed of an erbium-doped fiber [(EDF)-Thorlabs-M12-980-125] with a length of 10 m, a tunable laser source (TLS) at 1474 nm, and a WDM (1480/1550 nm) coupler. Then, the BP passes through the circulator and goes to the NZDSF with 25 km that acts as a Brillouin gain medium. This NZDSF has an effective area of $45.84 \mu\text{m}^2$, attenuation of 0.201 dB/km, and peak SBS efficiency of $0.2261 \text{ m}^{-1}\text{W}^{-1}$ at 1550 nm. This fiber was adopted in this study because it presents greater sensitivity to nonlinear effects when compared to standard SMFs due to its smaller core effective area.

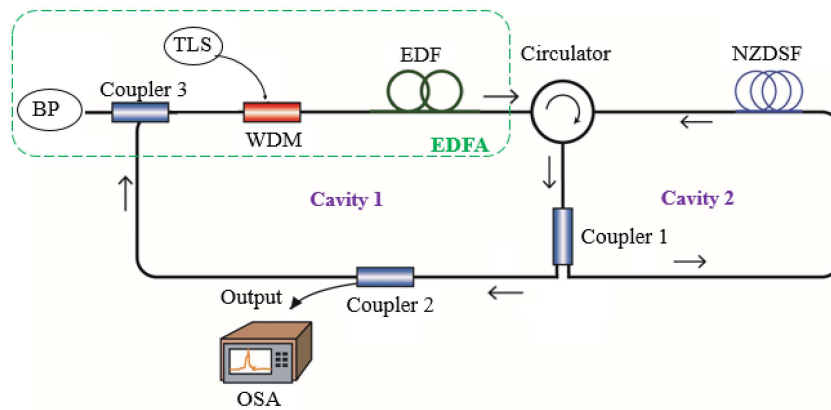


Figure 16 – Experimental setups for multi-wavelength ring cavity Brillouin fiber laser with a single frequency spacing configuration.

Once the BP signal goes to the Brillouin gain medium (NZDSF) a first Stokes signal is generated and it propagates in the backward direction. This first Stokes line passes through coupler 1, in which 90% of that power returns closing the loop, and 10% is directed to cavity 1. In coupler 2, 10% of the signal is displayed on the optical spectrum analyzer [(OSA) Anritsu MS9740A-009] with 30 pm resolution, and the other part is re-injected back into the EDFA as a new pump power through coupler 3 repeating the same path followed by the original BP, generating a new Stokes line with a Brillouin shift of 0.08 nm. This process continues until the higher-order Brillouin Stokes lines fall below the Brillouin threshold condition.

Figure 17 display the proposed MWBEFL with double frequency spacing. In this scheme two NZDSF are used as the Brillouin gain medium with a length of 25 km each, and also two EDFA gain blocks (EDFA 1 and EDFA 2). The EDFAs are again pumped through similar WDMs and pump lasers as used for single-frequency spacing laser shown in Figure 16. Three couplers (coupler 1, coupler 2, and coupler 3), with coupling ratios of 5/95, 5/95, and 50/50, respectively, and two circulators are used. The 1st Stokes line (S1) is generated at the NZDSF 1 and it propagated in the opposite direction of the BP with a frequency difference spacing of 0.08 nm, which can be seen at output 2, after circulator 1. The S1 then propagates to the NZDSF 2 through circulator 2 after amplification in EDFA 2, where the 2nd Stokes line (S2) is generated. The S2, now with a frequency spacing of 0.16 nm compared to the original BP is propagated through circulator 2 for visualization via a 5% port (output 1), and the remainder returns closing the cavity to become a new pump through coupler 3. After multiples rounds-trip, output 1 shows the odd Stokes components (S2, S4, S6,...), whereas the even Stokes components (S1, S3, S5,...) can be seen at output 2.

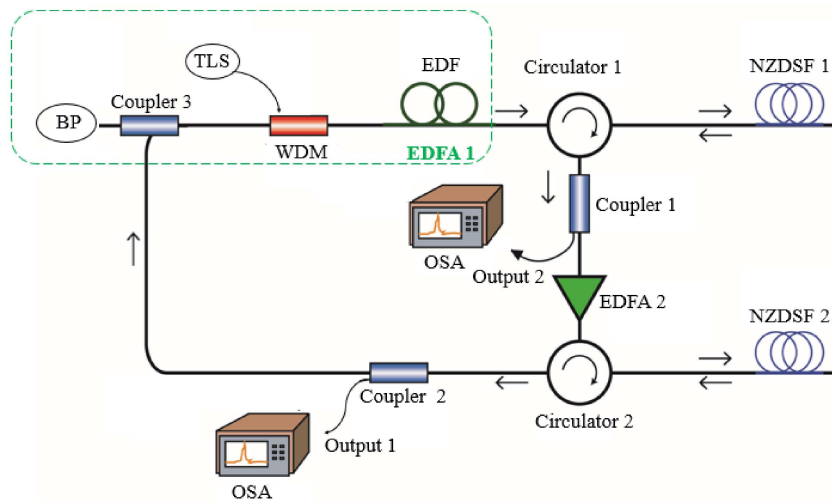


Figure 17 – Experimental setups for multi-wavelength ring cavity Brillouin fiber laser with a double frequency spacing configuration.

Finally, Figure 18 shows the experimental configuration proposed for the generation

of MWBEFL with triple frequency spacing. This setup is similar to the one proposed for the double frequency spacing laser. However, the first Stokes line generated in NZDSF 1 goes here through circulator 2 to cavity 2, which consists of the NZDSF 2, EDFA 2 and coupler 1. In this cavity, the second Stokes line is generated in an anticlockwise direction, and through coupler 1, 50% of the power of this Stokes line re-circulates inside this cavity and is amplified by EDFA 2 (with identical configuration to EDFA 1), at each round trip. In this process, a third Stokes line is generated in a backscattered direction, with a spacing of 0.24 nm in relation to the original BP. Then, this third Stokes line with triple frequency spacing propagates clockwise in the direction of coupler 1, where it is equally distributed between the cavities 1 and 2. The part of this power that arrives at coupler 2 is sent to the OSA via a 5% coupler port, and the rest returns as a new pump through coupler 3. In this way, new wavelengths with triple spacing are generated until the laser reaches saturation. In this last configuration, couplers 1, 2, and 3, have splittings ratios of 50/50, 5/95, and 50/50, respectively.

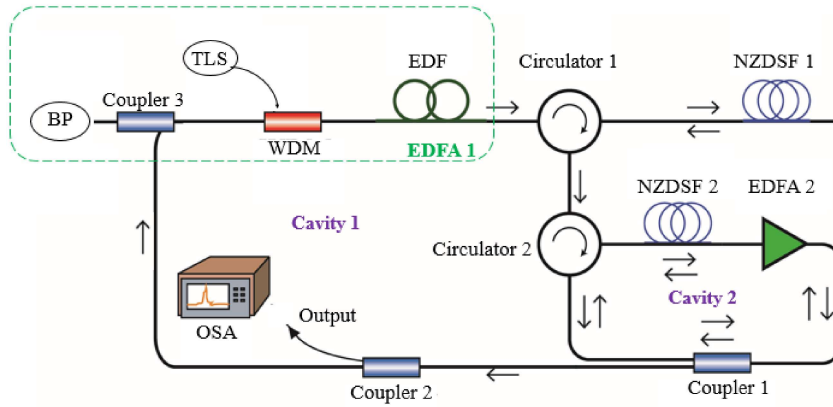


Figure 18 – Experimental setups for multi-wavelength ring cavity Brillouin fiber laser with a triple frequency spacing configuration.

4.2 Results and discussion

In this section, we present the results achieved from the proposed experimental setups for an MWBEFL. For a better presentation of these results, this section is divided into three subsections. The first one addresses the single frequency spacing configuration and presents an investigation of the laser performance concerning the number of Stokes lines generated. The following subsection describes the results of the double frequency spacing architecture. And the last one discusses the results of the triple frequency spacing arrangement.

4.2.1 Single frequency spacing Brillouin erbium fiber laser

The Figure 19 displays the MWBEFL with a single frequency spacing configuration. A total of 15 lasing lines, excluding the BP, were generated within a 30 dB range down

from the peak, as shown in Figure 19, with a total output power of 3.283 dBm. Lasing lines outside of this 30 dB range are not considered. The wavelength spacing between two adjacent lasing lines is 0.084 nm, which corresponds to a frequency shift of ~ 9.78 GHz at 1565.8 nm. The formation of anti-Stokes lines to the left of BP can be attributed to the interaction between the co-propagating BP power and the Stokes lines in the laser cavity through the four-wave mixing effect (AHMAD et al., 2020). Furthermore, from Figure 19, it can be observed that the BP is not as evident as compared to the other lasing lines. This could be attributed to the pump depletion after which the Brillouin gain starts to saturate. In addition, it is important to mention here that the residual power of the BP after its propagation in the fiber is discarded when it enters port 3 of the circulator.

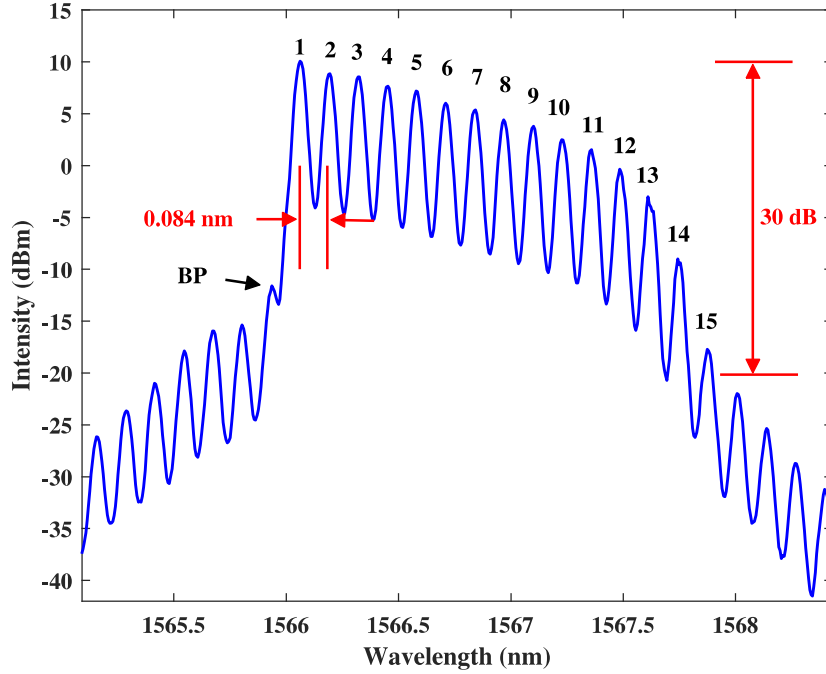


Figure 19 – Optical spectrum of the single Brillouin frequency spacing MWBEFL at the BP wavelength of 1565.8 nm and power of 1 mW. Here, the EDFA 1 pump power was 169.4 mW. Moreover, the frequency spacing between two adjacent wavelengths is 0.084 nm.

Figures 20, 21, and 22 display the optical spectra obtained with a single frequency spacing configuration when the parameters of EDFA (pump power) and BP (power and wavelength) are modified.

From the spectra presented in Figures 20 and 21 performer an analysis presented in Figure 23 that shows the number of generated Brillouin Stokes lines against the variations in EDFA pump power for BP wavelengths at 1565.8 nm and 1550.0 nm. It can be noted that the EDFA has greater efficiency in the 1565 nm spectral region, its can be explained due the self lasing cavity modes (erbium gain) in order to choose the BP wavelength that

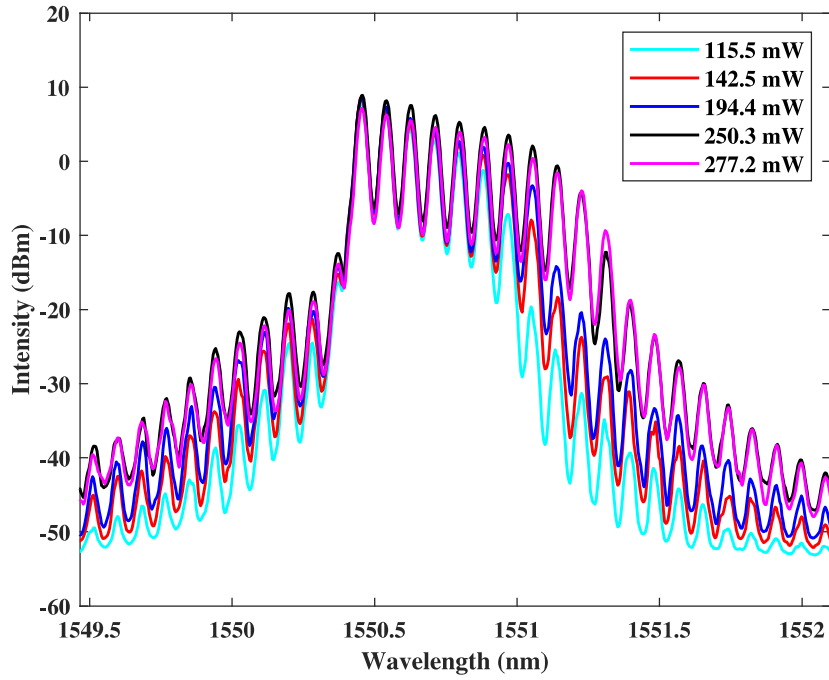


Figure 20 – Optical spectra generated with EDFA pump power values of 115.5 mW, 142.5 mW, 194.4 mW, 250.3 mW, and 277.2 mW. Here we adopt a BP power of 1 mW at 1550 nm.

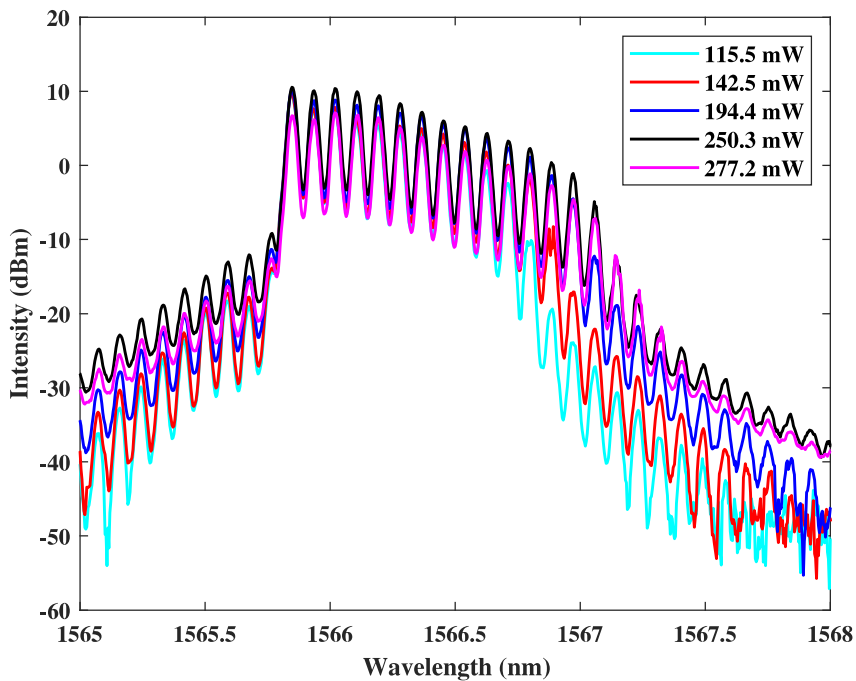


Figure 21 – Optical spectra generated with EDFA pump power values of 115.5 mW, 142.5 mW, 194.4 mW, 250.3 mW, and 277.2 mW. Here we adopt a BP power of 1 mW at 1565 nm.

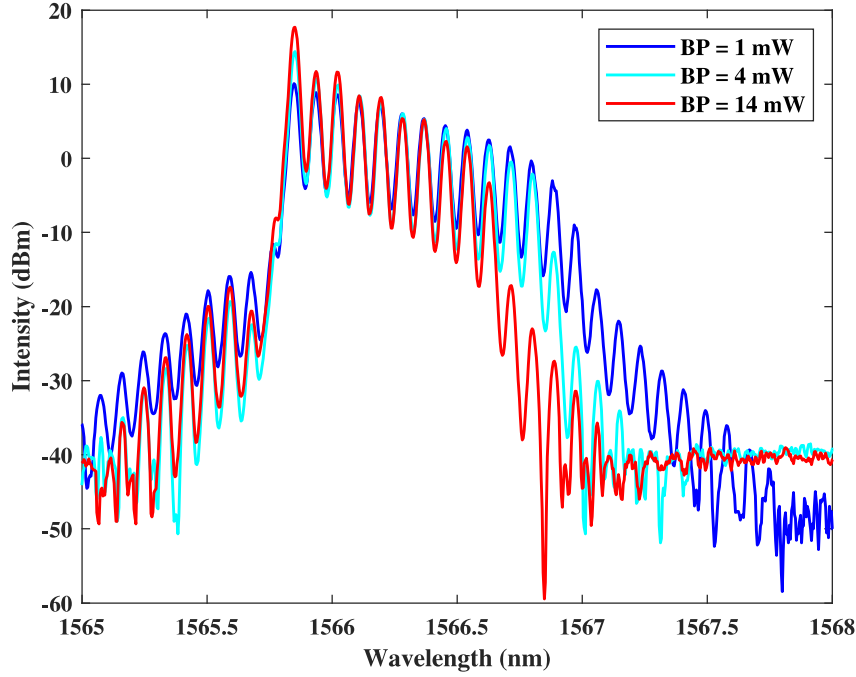


Figure 22 – Optical spectra generated with BP power values of 1 mW, 4 mW, and 14 mW. Here we adopt a EDFA pump power of 169 mW.

can get maximum gain inside the cavity, allowing the generation of up to 15 Stokes lines within a range of 30 dB down from the peak. In the region of 1550 nm 11 Stokes lines are generated in the same 30 dB range. BP wavelengths at 1527 nm and 1535 nm, were also evaluated. However, in these spectral regions, the EDFA exhibits a lower performance, generating a maximum of only 2 Stokes lines even for pump power around 250 mW.

Furthermore, the analysis of Figure 24 based on the spectra displayed in Figure 22, reveals that 1 mW of the BP power is more efficient in generating a greater number of Stokes lines than higher values of the BP, such as 4 mW or 14 mW when the EDFA pump power is fixed. This can be attributed to the fact that higher BP values force the EDFA to operate in a saturation regime so that its gain decreases for the new wavelengths generated, resulting in the reduction of the Stokes lines obtained. Besides, fixing the BP power, Figure 24 reveals that the number of Stokes lines grows with the increase of EDFA pump power from 115.5 mW to 169.4 mW. This increment on the EDFA output power leads to a higher circulating power inside of the laser cavity, which in its turn increases the Brillouin gain, leading to the increment of the number of Stokes lines generated.

4.2.2 Double frequency spacing Brillouin erbium fiber laser

Figures 25 and 26 exhibit the optical spectra obtained at outputs 1 and 2, respectively, with a double frequency spacing configuration formed due a multiples rounds-trip in

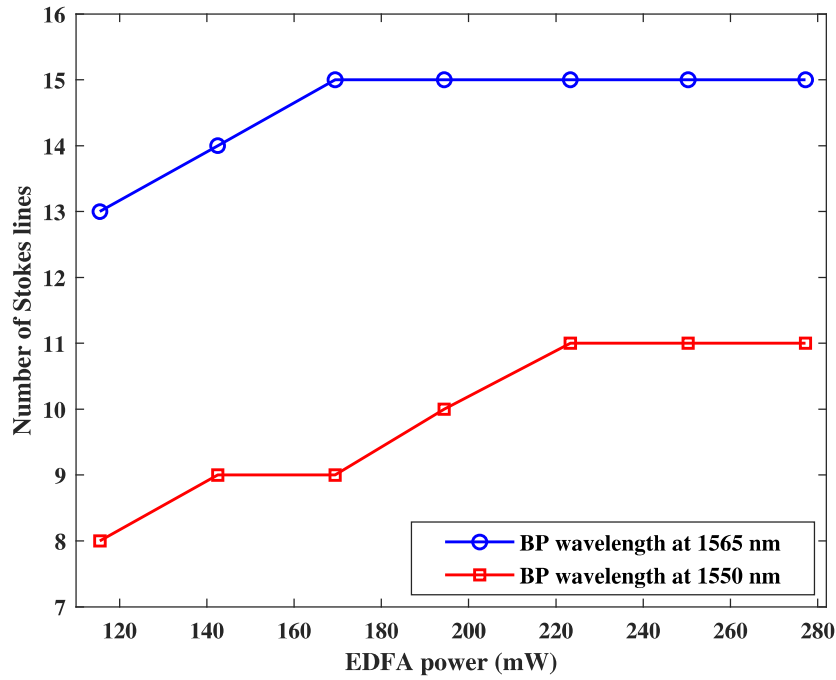


Figure 23 – Number of generated Brillouin Stokes lines within a range of 30 dB against the variations in EDFA pump power for BP wavelengths at 1565.8 nm and 1550.0 nm. Here we adopt a BP of 1 mW.

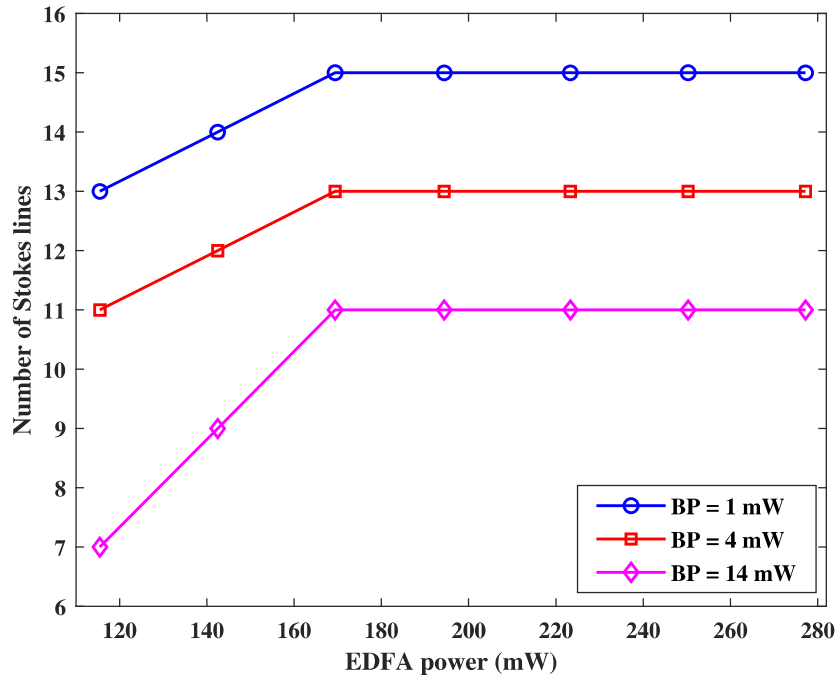


Figure 24 – Number of generated Brillouin Stokes lines within a range of 30 dB against the variations in EDFA pump power for BP powers of 1 mW, 4 mW, and 14 mW. Here we adopt all BP wavelengths at 1565.8 nm.

the laser cavity, show in 17. Based on the analyzes presented in the previous section, was set the BP wavelength at 1565.8 nm and with 1 mW of optical power. In this configuration, are employed two EDFAs (EDFA 1 and EDFA 2) both with pump powers of 336.5 mW. A total of 7 lasing lines (odd Stokes wavelengths) excluding the BP were generated at the output 1. At output 2, 7 lasing lines (even Stokes wavelengths) were generated. Both within a 30 dB range down from the peak and with an average OSNR as high as 30 dB. The total output powers at outputs 1 and 2 in this configuration were 2.764 dBm and 4.578 dBm, respectively. The wavelength spacing between two adjacent Stokes lines is 0.16 nm, which corresponds to a frequency shift of ~ 19.56 GHz at 1565.8 nm. It is important to emphasize here that if only 1 EDFA is employed, the number of Stokes lines drops by half within that same 30 dB range, which justifies incorporating the second EDFA. However, the addition of this second EDFA also causes a reduction of 1.9 dB in the OSNR observed, highlighted by the increase in the noise background.

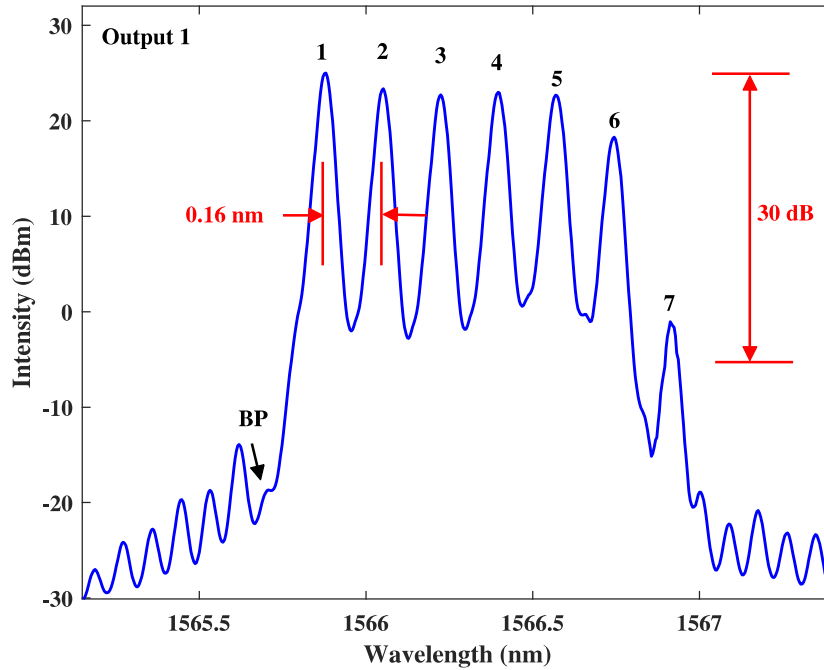


Figure 25 – Optical spectrum of the double Brillouin frequency spacing MWBEFL at the BP wavelength of 1565.8 nm, and power of 1 mW obtained at the output 1 (odd Stokes wavelengths). Here, the pump powers of EDFA 1 and EDFA 2 were both 336.5 mW. In addition, the frequency spacing between two adjacent wavelengths is 0.16 nm.

4.2.3 Triple frequency spacing Brillouin erbium fiber laser

For the end, was also investigate the performance of an MWBEFL with a triple frequency spacing configuration formed due to a three-times cascaded SBS in the laser cavity as shown in Figure 27. Again, the BP wavelength at 1565.8 nm and also using 1 mW

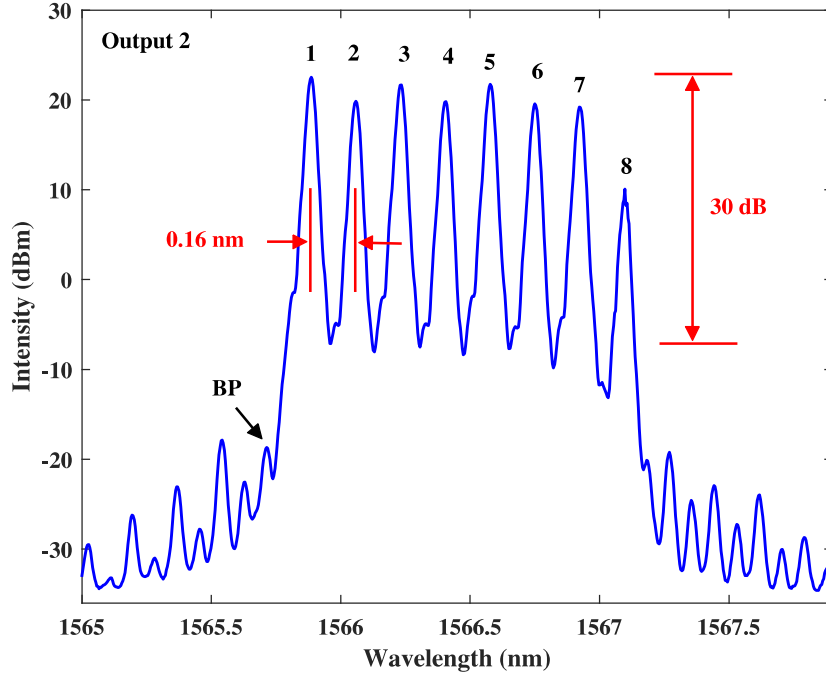


Figure 26 – Optical spectrum of the double Brillouin frequency spacing MWBEFL at the BP wavelength of 1565.8 nm, and power of 1 mW obtained at the output 2 (even Stokes wavelengths). Here, the pump powers of EDFA 1 and EDFA 2 were both 336.5 mW. Also, the frequency spacing between two adjacent wavelengths is 0.16 nm.

of optical power. Similar to the case of the double frequency spacing laser architecture, in this configuration, was employed two EDFAs (EDFA 1 and EDFA 2) both with pump powers of 336.5 mW. A total of 11 lasing lines excluding the BP were generated inside a 30 dB range with a total output power of - 4.948 dBm. The frequency spacing between two adjacent wavelengths is 0.24 nm, which corresponds to a frequency shift of ~ 29.12 GHz at 1565.8 nm. These signals with a frequency spacing of 29.12 GHz are the most promising candidates for the optical communications industry when compared to the signals generated with single and double frequency spacing configurations. This is due to the fact that this wider frequency shift not only facilitates the demultiplexing and filtering processes, but also allows for higher modulation rates to be applied to each channel without causing crosswalk effects. In this way, these type of lasers are strong candidates to be employed in dense wavelength division multiplexing communication systems.

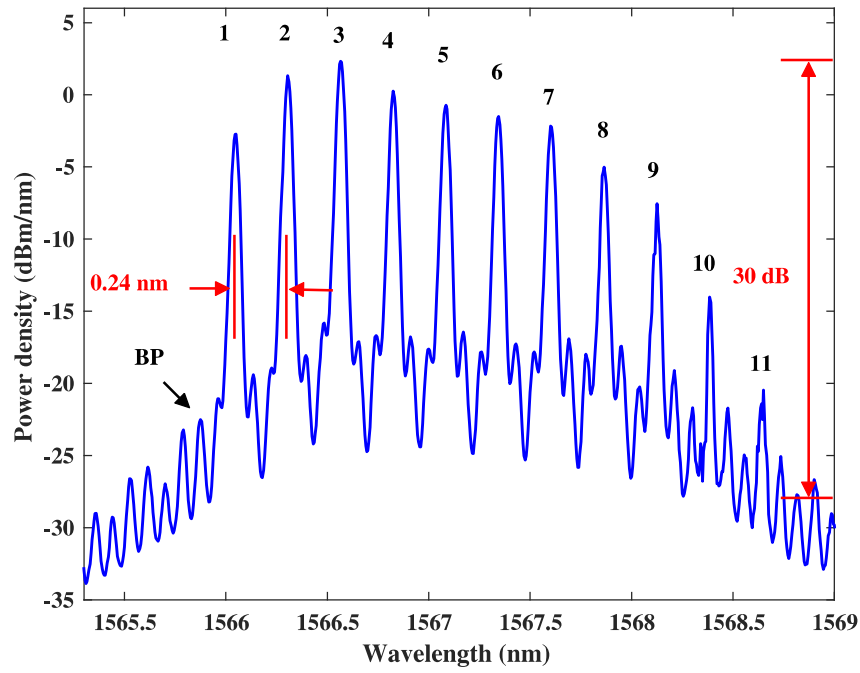


Figure 27 – Optical spectrum of the triple Brillouin frequency spacing MWBEFL at the BP wavelength of 1565.8 nm, and power of 1 mW. Here, the pump powers of EDFA 1 and EDFA 2 were both 336.5 mW. Further, the frequency spacing between two adjacent wavelengths is 0.24 nm.

5 Conclusions and future works

This dissertation presented the theoretical aspects and the experimental generation of multi-wavelength Brillouin fiber laser with single, double, and triple frequency spacing. This study is divided into two steps: a low threshold and highly efficient all-fiber Brillouin laser are done first, exploiting the Brillouin amplification effect, and then using the Brillouin cascaded method for the generated multiples wavelength with different spacing frequencies in an all-fiber configuration.

Foremost, was experimentally demonstrated in an simple and compact all fiber configuration stable Brillouin fiber lasers using three different types of optical fibers. Thresholds as low as 1.15 mW and efficiencies as high as 49.43% could be obtained. The performance of those lasers were analyzed by changing the output coupler from a 10 to 90% ratio and an OSA with a 1.12 pm resolution was used to analyze differences in spectral shifts. Due to low resonator loss, a relatively low pump threshold, very small linewidth, and a simple configuration Brillouin lasers can potentially be adapted for applications such as optical sensing (due to the temperature dependence of the Brillouin shift can be used for temperature and pressure sensing) and comb generation.

Therefore, is demonstrated by the generation of multi-wavelength fiber lasers operating in the 1.5 μm spectral region with three different frequency spacing architectures at a low threshold. The combination of a fiber with high non-linearity that enables a sizeable Brillouin gain, with compact all-fiber setups that allow shallow intracavity losses, in addition to the use of a very narrow linewidth laser source has successfully generated 15, 15 (totaling the two outputs), and 11 Stokes channels in single, double and triple frequency spacing configurations, respectively, with a BP power as low as 1 mW. These laser sources can be applied not only in dense wavelength division multiplexing communication operations, but also in the sensing field.

Possible future work consists in optimizing the fiber and laser parameters, with the support of numerical/analytical simulations in order to enhance the number of generated wavelengths and also their flatness. Additionally, future works include building similar laser systems employing highly nonlinear special fiber types, such as perfluorinated polymer optical fiber as the Brillouin gain medium, which should enable the generation of a multiple wavelength laser with different values of frequency spacing shift, and apply in the sensors field.

Bibliography

AGRAWAL, G. P. Nonlinear fiber optics. In: *Nonlinear Science at the Dawn of the 21st Century*. [S.l.]: Springer, 2000. p. 195–211. Citado 8 vezes nas páginas [18](#), [19](#), [20](#), [22](#), [35](#), [40](#), [43](#), and [44](#).

AGRAWAL, G. P. *Fiber-optic communication systems*. [S.l.]: John Wiley & Sons, 2012. Citado na página [19](#).

AGRELL, E. et al. Roadmap of optical communications. *Journal of Optics*, IOP Publishing, v. 18, n. 6, p. 1–40, 2016. Citado na página [30](#).

AHMAD, H. et al. Multiwavelength Brillouin Generation in Bismuth-Doped Fiber Laser With Single-and Double-Frequency Spacing. *Journal of Lightwave Technology*, OSA, v. 38, n. 24, p. 6886–6896, 2020. Citado na página [54](#).

AL-ALIMI, A. et al. Stable multiwavelength thulium fiber laser assisted by four wave mixing effect. *Optics & Laser Technology*, Elsevier, v. 106, p. 191–196, 2018. Citado na página [30](#).

AL-ALIMI, A. et al. Wide bandwidth and flat multiwavelength Brillouin-erbium fiber laser. *Optics express*, Optical Society of America, v. 25, n. 16, p. 19382–19390, 2017. Citado na página [31](#).

AL-MASHHADANI, M. K. S.; AL-MASHHADANI, T. F.; GOKTAS, H. H. Broadly tunable 40 ghz brillouin frequency spacing multiwavelength brillouin–erbium fiber laser for dwdm. *Optics Communications*, Elsevier, v. 451, p. 116–123, 2019. Citado na página [18](#).

AL-MASHHADANI, M. K. S.; AL-MASHHADANI, T. F.; GOKTAS, H. H. Broadly tunable 40 GHz Brillouin frequency spacing multiwavelength Brillouin-Erbium fiber laser for DWDM. *Optics Communications*, Elsevier, v. 451, p. 116–123, 2019. Citado na página [19](#).

AL-MASHHADANI, M. K. S.; AL-MASHHADANI, T. F.; GOKTAS, H. H. Tunable 50 GHz laser comb generation of multiwavelength Brillouin erbium fiber laser. *Optics Communications*, Elsevier, v. 464, p. 1–7, 2020. Citado na página [19](#).

ARNON, S.; KOPEIKA, N. S. Laser satellite communication network-vibration effect and possible solutions. *Proceedings of the IEEE*, IEEE, v. 85, n. 10, p. 1646–1661, 1997. Citado na página [30](#).

ASTAPOVICH, M. S. et al. Watt-level nanosecond 4.42- μ m raman laser based on silica fiber. *IEEE Photonics Technology Letters*, IEEE, v. 31, n. 1, p. 78–81, 2018. Citado na página [32](#).

BAHRAMI, H. et al. 16-wavelength dwdm a-rof with stimulated brillouin scattering suppression, for antenna remotng in wireless front-haul. In: IEEE. *2018 International Topical Meeting on Microwave Photonics (MWP)*. [S.l.], 2018. p. 1–4. Citado na página [32](#).

BAIRD, J. British patent specification no. 20969/27. *HM Patents Office*, 1927. Citado na página [19](#).

BERGER, M. S. *Nonlinearity and functional analysis: lectures on nonlinear problems in mathematical analysis*. [S.l.]: Academic press, 1977. v. 74. Citado na página [32](#).

BERGLER, M. et al. Cooling rate calibration and mapping of ultra-short pulsed laser modifications in fused silica by raman and brillouin spectroscopy. *International Journal of Extreme Manufacturing*, IOP Publishing, v. 2, n. 3, p. 035001, 2020. Citado na página [18](#).

BIANCHETTI, M. et al. Switchable multi-wavelength laser based on a core-offset Mach-Zehnder interferometer with non-zero dispersion-shifted fiber. *Optics & Laser Technology*, Elsevier, v. 104, p. 49–55, 2018. Citado na página [30](#).

BOYD, R. W. *Nonlinear optics*. [S.l.]: Academic press, 2020. Citado 11 vezes nas páginas [24](#), [25](#), [31](#), [32](#), [36](#), [37](#), [39](#), [40](#), [41](#), [42](#), and [43](#).

DAJANI, I. et al. Stimulated brillouin scattering suppression through laser gain competition: scalability to high power. *Optics Letters*, Optical Society of America, v. 35, n. 18, p. 3114–3116, 2010. Citado na página [18](#).

DESURVIRE, E.; ZERVAS, M. N. Erbium-doped fiber amplifiers: principles and applications. *Physics Today*, v. 48, n. 2, p. 56, 1995. Citado na página [29](#).

DIAMANDI, H. H.; ZADOK, A. Ultra-narrowband integrated brillouin laser. *Nature Photonics*, Nature Publishing Group, v. 13, n. 1, p. 9–10, 2019. Citado na página [18](#).

DIGONNET, M. J. *Rare-earth-doped fiber lasers and amplifiers, revised and expanded*. [S.l.]: CRC press, 2001. Citado na página [18](#).

DONALDSON, K. E. et al. Femtosecond laser-assisted cataract surgery. *Journal of Cataract & Refractive Surgery*, Elsevier, v. 39, n. 11, p. 1753–1763, 2013. Citado na página [30](#).

DONG, Y. High-performance distributed brillouin optical fiber sensing. *Photonic Sensors*, Springer, v. 11, n. 1, p. 69–90, 2021. Citado na página [18](#).

EL-DESSOUKY, H. et al. *High Performance Textiles and their Application*, C. Lawrence. [S.l.]: Woodhead Publishing Ltd., UK, 2014. Citado na página [28](#).

ERINGEN, A. C. *Mechanics of continua*. *Huntington*, 1980. Citado na página [38](#).

FABELINSKII, I. L. *Molecular scattering of light*. [S.l.]: Springer Science & Business Media, 2012. Citado na página [25](#).

FENG, T. et al. High stability multiwavelength random erbium-doped fiber laser with a reflecting-filter of six-superimposed fiber-Bragg-gratings. *OSA Continuum*, Optical Society of America, v. 2, n. 9, p. 2526–2538, 2019. Citado na página [30](#).

FENG, X.; TAM, H.-y.; WAI, P. K. A. Stable and uniform multiwavelength erbium-doped fiber laser using nonlinear polarization rotation. *Optics express*, Optica Publishing Group, v. 14, n. 18, p. 8205–8210, 2006. Citado na página [18](#).

- FENG, X.; TAM, H. yaw; WAI, P. K. A. Stable and uniform multiwavelength erbium-doped fiber laser using nonlinear polarization rotation. *Optics Express*, OSA, v. 14, n. 18, p. 8205–8210, 2006. Citado na página 30.
- FOTIOU, I. A.; PARRILO, P. A.; MORARI, M. Nonlinear parametric optimization using cylindrical algebraic decomposition. In: IEEE. *Proceedings of the 44th IEEE Conference on Decision and Control*. [S.l.], 2005. p. 3735–3740. Citado na página 32.
- FOX, M. *Optical properties of solids*. [S.l.]: American Association of Physics Teachers, 2002. Citado na página 25.
- FREUDIGER, C. W. et al. Stimulated raman scattering microscopy with a robust fibre laser source. *Nature photonics*, Nature Publishing Group, v. 8, n. 2, p. 153–159, 2014. Citado na página 18.
- FRIEDLI, P. et al. Four-wave mixing in a quantum cascade laser amplifier. *Applied Physics Letters*, American Institute of Physics, v. 102, n. 22, p. 222104, 2013. Citado na página 18.
- F.R.S., J. T. P. I. on the vibrations and tones produced by the contact of bodies having different temperatures. *The London, Edinburgh, and Dublin Philosophical Magazine and Journal of Science*, Taylor Francis, v. 8, p. 1–12, 1854. Disponível em: <<https://doi.org/10.1080/14786445408651882>>. Citado na página 19.
- FU, J. et al. A novel-configuration multi-wavelength Brillouin erbium fiber laser and its application in switchable high-frequency microwave generation. *Laser physics*, Springer, v. 20, n. 10, p. 1907–1912, 2010. Citado na página 30.
- GALINDO-SANTOS, J. et al. Brillouin filtering of optical combs for narrow linewidth frequency synthesis. *Optics Communications*, Elsevier, v. 366, p. 33–37, 2016. Citado na página 31.
- GILES, C. Lightwave applications of fiber bragg gratings. *Journal of lightwave technology*, IEEE, v. 15, n. 8, p. 1391–1404, 1997. Citado na página 18.
- GLOGE, D. Weakly guiding fibers. *Applied optics*, Optica Publishing Group, v. 10, n. 10, p. 2252–2258, 1971. Citado na página 21.
- HAN, T.; WU, G.; LU, Y. Crack monitoring using short-gauged brillouin fiber optic sensor. *Measurement*, Elsevier, v. 179, p. 109461, 2021. Citado na página 32.
- HAN, Y.-G. et al. Multiwavelength Raman-fiber-laser-based long-distance remote sensor for simultaneous measurement of strain and temperature. *Optics Letters*, OSA, v. 30, n. 11, p. 1282–1284, 2005. Citado na página 30.
- HE, W. et al. C-band switchable multi-wavelength erbium-doped fiber laser based on Mach-Zehnder interferometer employing seven-core fiber. *Optical Fiber Technology*, Elsevier, v. 46, p. 30–35, 2018. Citado na página 30.
- HECHT, J. Illuminating the origin of light guiding. *Optics and Photonics News*, Optica Publishing Group, v. 10, n. 10, p. 26, 1999. Citado na página 19.
- HECHT, J. *City of light: the story of fiber optics*. [S.l.]: Oxford University Press on Demand, 2004. Citado 3 vezes nas páginas 18, 27, and 34.

- HECHT, J. *Understanding fiber optics*. [S.l.]: Jeff Hecht, 2015. Citado 2 vezes nas páginas 25 and 28.
- HEEL, A. C. van. A new method of transporting optical images without aberrations. *Nature*, Nature Publishing Group, v. 173, n. 4392, p. 39–39, 1954. Citado na página 19.
- HEIMAN, D.; HAMILTON, D.; HELLWARTH, R. Brillouin scattering measurements on optical glasses. *Physical Review B*, APS, v. 19, n. 12, p. 6583, 1979. Citado na página 45.
- HU, T.; JACKSON, S. D.; HUDSON, D. D. Ultrafast pulses from a mid-infrared fiber laser. *Optics letters*, Optical Society of America, v. 40, n. 18, p. 4226–4228, 2015. Citado na página 18.
- JAUREGUI, C.; LIMPET, J.; TÜNNERMANN, A. High-power fibre lasers. *Nature photonics*, Nature Publishing Group, v. 7, n. 11, p. 861–867, 2013. Citado na página 18.
- JEON, H.-b.; LEE, H. Photonic true-time delay for phased-array antenna system using dispersion compensating module and a multiwavelength fiber laser. *Journal of the Optical Society of Korea*, Optical Society of Korea, v. 18, n. 4, p. 406–413, 2014. Citado na página 30.
- JR, P. C. D.; FRAGNITO, H. Espalhamento brillouin em fibra fotônicas. *Universidade Estadual de Campinas, Tese Doutorado*, 2006. Citado 4 vezes nas páginas 25, 34, 39, and 46.
- KAO, K. C.; HOCKHAM, G. A. Dielectric-fibre surface waveguides for optical frequencies. In: IET. *Proceedings of the Institution of Electrical Engineers*. [S.l.], 1966. v. 113, n. 7, p. 1151–1158. Citado na página 20.
- KAPANY, N. Fiber optics. principles and applications. *New York: Academic Press*, 1967. Citado na página 20.
- KAPRON, F.; KECK, D. B.; MAURER, R. D. Radiation losses in glass optical waveguides. *Applied Physics Letters*, American Institute of Physics, v. 17, n. 10, p. 423–425, 1970. Citado na página 20.
- KAUSHAL, H.; KADDOUM, G. Applications of lasers for tactical military operations. *IEEE Access*, IEEE, v. 5, p. 20736–20753, 2017. Citado na página 30.
- KEISER, G. E. A review of wdm technology and applications. *Optical Fiber Technology*, Elsevier, v. 5, n. 1, p. 3–39, 1999. Citado na página 29.
- KEMAL, J. N. et al. Multi-wavelength coherent transmission using an optical frequency comb as a local oscillator. *Optics express*, Optical Society of America, v. 24, n. 22, p. 25432–25445, 2016. Citado na página 30.
- LACRAZ, A. et al. Femtosecond laser inscribed bragg gratings in low loss cytop polymer optical fiber. *IEEE Photonics Technology Letters*, IEEE, v. 27, n. 7, p. 693–696, 2015. Citado na página 18.
- LANDAU, L. D.; LIFSHITZ, E. M. *Fluid Mechanics: Landau and Lifshitz: Course of Theoretical Physics, Volume 6*. [S.l.]: Elsevier, 2013. v. 6. Citado na página 34.

- LI, Y. et al. Tunable multiwavelength fiber laser based on a θ -shaped microfiber filter. *Applied Physics B*, Springer, v. 124, n. 6, p. 1–6, 2018. Citado na página 30.
- LIAN, Y. et al. Multiwavelength fiber laser using erbium-doped twin-core fiber and nonlinear optical loop mirror. *IEEE Access*, IEEE, v. 7, p. 152478–152482, 2019. Citado na página 30.
- LIEW, S. H. Laser hair removal. *American journal of clinical dermatology*, Springer, v. 3, n. 2, p. 107–115, 2002. Citado na página 30.
- LIU, Y. et al. Triple brillouin frequency spacing brillouin fiber laser sensor for temperature measurement. *Optical Fiber Technology*, Elsevier, v. 54, p. 102106, 2020. Citado na página 18.
- LIU, Y.-g.; WANG, D.; DONG, X. Stable room-temperature multi-wavelength lasing oscillations in a Brillouin-Raman fiber ring laser. *Optics Communications*, Elsevier, v. 281, n. 21, p. 5400–5404, 2008. Citado na página 31.
- MAMDOOHI, G. et al. Switchable multiwavelength Brillouin-Raman fiber laser utilizing an enhanced nonlinear amplifying fiber loop design. *IEEE Photonics Journal*, IEEE, v. 10, n. 2, p. 1–11, 2018. Citado na página 30.
- MARINI, D. et al. Botda sensing employing a modified brillouin fiber laser probe source. *Journal of Lightwave Technology*, IEEE, v. 36, n. 4, p. 1131–1137, 2017. Citado na página 18.
- MARSHALL, J.; STEWART, G.; WHITENETT, G. Design of a tunable L-band multi-wavelength laser system for application to gas spectroscopy. *Measurement Science and Technology*, IOP Publishing, v. 17, n. 5, p. 1023–1031, 2006. Citado na página 30.
- MEARS, R. The edfa: past, present and future. In: IEEE. *Fifth Asia-Pacific Conference on... and Fourth Optoelectronics and Communications Conference on Communications*, [S.l.], 1999. v. 2, p. 1332–vol. Citado na página 28.
- MIYA, T. et al. Ultimate low-loss single-mode fibre at 1.55 μ m. *Electronics Letters*, v. 4, n. 15, p. 106–108, 1979. Citado na página 20.
- MIZUNO, Y. et al. Noise suppression technique for distributed brillouin sensing with polymer optical fibers. *Optics Letters*, Optical Society of America, v. 44, n. 8, p. 2097–2100, 2019. Citado na página 18.
- MOON, D. S. et al. Tunable multi-wavelength SOA fiber laser based on a Sagnac loop mirror using an elliptical core side-hole fiber. *Optics Express*, OSA, v. 15, n. 13, p. 8371–8376, 2007. Citado na página 30.
- MOZAFFARI, M. H.; FARMANI, A. On-chip single-mode optofluidic microresonator dye laser sensor. *IEEE Sensors Journal*, IEEE, v. 20, n. 7, p. 3556–3563, 2019. Citado na página 27.
- NAKAZAWA, M.; KIMURA, Y.; SUZUKI, K. Efficient er3+-doped optical fiber amplifier pumped by a 1.48 μ m ingaasp laser diode. *Applied physics letters*, American Institute of Physics, v. 54, n. 4, p. 295–297, 1989. Citado na página 28.

- NASIR, M. M. et al. Broadly tunable multi-wavelength Brillouin-erbium fiber laser in a Fabry-Perot cavity. *Laser Physics Letters*, Wiley Online Library, v. 5, n. 11, p. 812–816, 2008. Citado na página 31.
- OH, W.-Y. et al. 10 and 20 GHz optical combs generation in Brillouin/erbium fiber laser with shared cavity of Sagnac reflector. *Optics communications*, Elsevier, v. 201, n. 4-6, p. 399–403, 2002. Citado na página 31.
- OKOSHI, T. *Optical fibers*. [S.l.]: Elsevier, 2012. Citado 2 vezes nas páginas 23 and 24.
- OLSSON, N.; ZIEL, J. Van der. Cancellation of fiber loss by semiconductor laser pumped brillouin amplification at 1.5 μm . *Applied physics letters*, American Institute of Physics, v. 48, n. 20, p. 1329–1330, 1986. Citado na página 44.
- OTTERSTROM, N. T. et al. A silicon brillouin laser. *Science*, American Association for the Advancement of Science, v. 360, n. 6393, p. 1113–1116, 2018. Citado na página 18.
- PAN, S.; LOU, C.; GAO, Y. Multiwavelength erbium-doped fiber laser based on inhomogeneous loss mechanism by use of a highly nonlinear fiber and a Fabry-Perot filter. *Optics Express*, OSA, v. 14, n. 3, p. 1113–1118, 2006. Citado na página 30.
- PARVIZI, R. et al. 0.16 nm spaced multi-wavelength Brillouin fiber laser in a figure-of-eight configuration. *Optics & Laser Technology*, Elsevier, v. 43, n. 4, p. 866–869, 2011. Citado na página 31.
- PASCHOTTA, R. *Encyclopedia of laser physics and technology*. [S.l.]: Wiley-vch, 2008. v. 1. Citado na página 20.
- PAYNE, D. et al. Low noise erbium doped fiber amplifier operating at 1.54 μm . *Electronic Letters*, v. 23, n. 19, p. 1026–1027, 1987. Citado na página 29.
- PELUSI, M.; INOUE, T.; NAMIKI, S. Enhanced carrier to noise ratio by brillouin amplification for optical communications. *Journal of Lightwave Technology*, IEEE, v. 38, n. 2, p. 319–331, 2019. Citado na página 18.
- PENG, W. et al. Tunable self-seeded multiwavelength brillouin–erbium fiber laser using an in-line two-taper mach–zehnder interferometer. *Optics & Laser Technology*, Elsevier, v. 45, p. 348–351, 2013. Citado na página 19.
- QUIMBY, R. S. *Photonics and lasers: an introduction*. [S.l.]: John Wiley & Sons, 2006. Citado na página 30.
- SALEH, B. E.; TEICH, M. C. *Fundamentals of photonics*. [S.l.]: John Wiley & sons, 2019. Citado na página 27.
- SCHULTE, J. et al. Nonlinear pulse compression in a multi-pass cell. *Optics Letters*, Optical Society of America, v. 41, n. 19, p. 4511–4514, 2016. Citado na página 32.
- SHAO, Z.-K. et al. A high-performance topological bulk laser based on band-inversion-induced reflection. *Nature nanotechnology*, Nature Publishing Group, v. 15, n. 1, p. 67–72, 2020. Citado na página 27.
- SHEE, Y. et al. Multiwavelength Brillouin-erbium fiber laser with double-Brillouin-frequency spacing. *Optics express*, Optical Society of America, v. 19, n. 3, p. 1699–1706, 2011. Citado na página 31.

- SHIRAZI, M. R. et al. A linear cavity Brillouin fiber laser with multiple wavelengths output. *Laser Physics Letters*, Wiley Online Library, v. 5, n. 5, p. 361–363, 2008. Citado na página 31.
- SILFVAST, W. T. *Laser fundamentals*. [S.l.]: Cambridge university press, 2004. Citado 2 vezes nas páginas 27 and 30.
- SILVA, L. C.; CASTELLANI, C. E. Numerical analysis of the pump's spectral linewidth impact on single and multi-wavelength brillouin fiber lasers. *Laser Physics*, IOP Publishing, v. 31, n. 5, p. 055104, 2021. Citado na página 45.
- SNYDER, A. W.; LOVE, J. *Optical waveguide theory*. [S.l.]: Springer Science & Business Media, 2012. Citado na página 21.
- SPRANGLE, P. et al. High-power lasers for directed-energy applications. *Applied optics*, Optica Publishing Group, v. 54, n. 31, p. F201–F209, 2015. Citado na página 18.
- TIU, Z. C. et al. Single and double Brillouin frequency spacing multi-wavelength Brillouin erbium fiber laser with micro-air gap cavity. *IEEE Journal of Quantum Electronics*, IEEE, v. 52, n. 9, p. 1–5, 2016. Citado na página 31.
- TRAXER, O.; KELLER, E. X. Thulium fiber laser: the new player for kidney stone treatment? a comparison with holmium: Yag laser. *World journal of urology*, Springer, v. 38, n. 8, p. 1883–1894, 2020. Citado na página 27.
- WANG*, G.; XIE, S. Optimal process planning for a combined punch-and-laser cutting machine using ant colony optimization. *International Journal of Production Research*, Taylor & Francis, v. 43, n. 11, p. 2195–2216, 2005. Citado na página 30.
- WANG, X. et al. Tunable multiwavelength narrow linewidth Brillouin erbium fiber laser based on Rayleigh backscattering. *Optical Engineering*, International Society for Optics and Photonics, v. 55, n. 6, p. 1–6, 2016. Citado na página 31.
- WANG, X. et al. Multiwavelength brillouin-thulium fiber laser. *IEEE Photonics Journal*, IEEE, v. 6, n. 1, p. 1–7, 2013. Citado na página 18.
- WANG, Z. et al. Broadband flat-amplitude multiwavelength Brillouin-Raman fiber laser with spectral reshaping by Rayleigh scattering. *Optics express*, Optical Society of America, v. 21, n. 24, p. 29358–29363, 2013. Citado na página 31.
- XING, S. et al. Mid-infrared continuous-wave parametric amplification in chalcogenide microstructured fibers. *Optica*, Optica Publishing Group, v. 4, n. 6, p. 643–648, 2017. Citado na página 18.
- XU, R.; YUAN, L.; ZHANG, X. Multiwavelength brillouin-erbium fiber laser with quadruple-brillouin-frequency spacing. In: OPTICA PUBLISHING GROUP. *Optical Fiber Sensors*. [S.l.], 2018. p. WF52. Citado na página 18.
- XUEFANG, Z. et al. Multi-wavelength brillouin erbium-doped fiber laser sensor with high tunable temperature sensing coefficient. *Optical and Quantum Electronics*, Springer, v. 51, n. 1, p. 1–14, 2019. Citado na página 18.

YAO, S. et al. Few-mode fiber Bragg grating-based multi-wavelength fiber laser with tunable orbital angular momentum beam output. *Laser Physics Letters*, IOP Publishing, v. 15, n. 9, p. 1–6, 2018. Citado na página 30.

YEOM, D.-I. et al. Low-threshold supercontinuum generation in highly nonlinear chalcogenide nanowires. *Optics letters*, Optica Publishing Group, v. 33, n. 7, p. 660–662, 2008. Citado na página 32.

YÜCEL, M. et al. Experimental analysis of the temperature dependence of the brillouin gain spectrum in short-length single-mode fiber. *Turkish Journal of Electrical Engineering and Computer Sciences*, v. 25, n. 5, p. 3881–3891, 2017. Citado 2 vezes nas páginas 11 and 35.

ZHANG, L. et al. Multiwavelength coherent Brillouin random fiber laser with ultrahigh optical signal-to-noise ratio. *IEEE Journal of Selected Topics in Quantum Electronics*, IEEE, v. 24, n. 3, p. 1–8, 2017. Citado na página 30.

ZHANG, L. et al. Multi-wavelength brillouin random fiber laser via distributed feedback from a random fiber grating. *Journal of Lightwave Technology*, IEEE, v. 36, n. 11, p. 2122–2128, 2018. Citado na página 18.

ZHANG, Q. et al. Halide perovskite semiconductor lasers: materials, cavity design, and low threshold. *Nano Letters*, ACS Publications, v. 21, n. 5, p. 1903–1914, 2021. Citado na página 27.

ZHANG, Z.; ZHAN, L.; XIA, Y. Tunable self-seeded multiwavelength brillouin-erbium fiber laser with enhanced power efficiency. *Optics Express*, Optica Publishing Group, v. 15, n. 15, p. 9731–9736, 2007. Citado na página 19.

ZHAO, Q. et al. Wide tuning range and high OSNR self-seeded multi-wavelength Brillouin-erbium fiber laser based on a Lyot filter. *Applied Optics*, Optical Society of America, v. 57, n. 36, p. 10474–10479, 2018. Citado na página 30.

ZHONG, K. et al. Digital signal processing for short-reach optical communications: A review of current technologies and future trends. *Journal of Lightwave Technology*, IEEE, v. 36, n. 2, p. 377–400, 2018. Citado na página 30.

ZHOU, X. et al. An L-band multi-wavelength Brillouin-erbium fiber laser with switchable frequency spacing. *Laser Physics*, IOP Publishing, v. 27, n. 1, p. 1–5, 2016. Citado na página 31.

ZHOU, Z. et al. High-power tunable mid-infrared fiber gas laser source by acetylene-filled hollow-core fibers. *Optics Express*, Optica Publishing Group, v. 26, n. 15, p. 19144–19153, 2018. Citado na página 27.